Article

Cell Metabolism

Efferocytosis induces macrophage proliferation to help resolve tissue injury

Graphical abstract

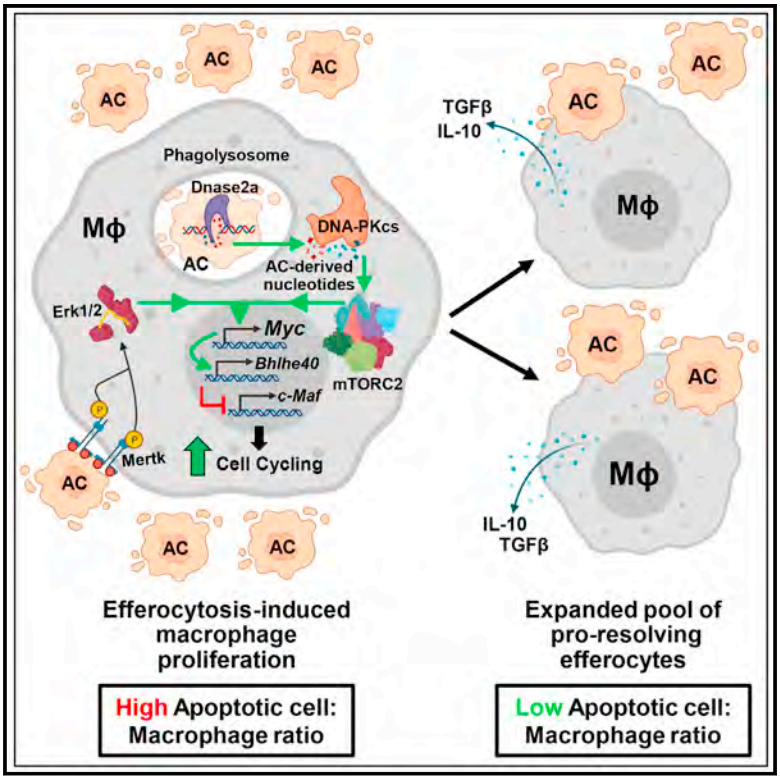

Highlights

- Apoptotic cell degradation after macrophage efferocytosis induces proliferation
- Apoptotic cell-derived nucleotides trigger a DNA-PK-mTorc2-Myc proliferation pathway
- Proliferating efferocytic macrophages are pro-resolving *in vitro* and *in vivo*
- Genetic silencing of the proliferation pathway hinders atherosclerosis regression

Authors

Brennan D. Gerlach, Patrick B. Ampomah, Arif Yurdagul, Jr., ..., Jinjun Shi, Wei Tao, Ira Tabas

Correspondence

iat1@cumc.columbia.edu

In brief

Apoptotic cell (AC) clearance by macrophages (efferocytosis) promotes tissue resolution, and its failure contributes to inflammatory diseases. Gerlach et al. show that AC-nucleotides trigger efferocytosing macrophages to proliferate, which is essential for resolution *in vivo*, including in atherosclerosis regression. These findings may suggest new ways to treat non-resolving inflammatory diseases.

Gerlach et al., 2021, Cell Metabolism *33*, 2445–2463
December 7, 2021
https://doi.org/10.1016/j.cmet.2021.10.015

CellPress

Cell Metabolism

CellPress

Article

Efferocytosis induces macrophage proliferation to help resolve tissue injury

Brennan D. Gerlach,[1,5,7] Patrick B. Ampomah,[1,7] Arif Yurdagul, Jr.,[1,6] Chuang Liu,[2] Max C. Lauring,[1] Xiaobo Wang,[1] Canan Kasikara,[1] Na Kong,[2] Jinjun Shi,[2] Wei Tao,[2] and Ira Tabas[1,3,4,8,*]

[1]Department of Medicine, Columbia University Irving Medical Center, New York, NY 10032, USA
[2]Center for Nanomedicine and Department of Anesthesiology, Brigham and Women's Hospital, Harvard Medical School, Boston, MA 02115, USA
[3]Department of Pathology and Cell Biology, Columbia University Irving Medical Center, New York, NY 10032, USA
[4]Department of Physiology, Columbia University Irving Medical Center, New York, NY 10032, USA
[5]Present address: Novartis Institutes for BioMedical Research, Cambridge, MA 02139, USA
[6]Present address: Department of Molecular and Cellular Physiology, LSU Health Shreveport, Shreveport, LA 71130, USA
[7]These authors contributed equally
[8]Lead contact
*Correspondence: iat1@cumc.columbia.edu
https://doi.org/10.1016/j.cmet.2021.10.015

SUMMARY

Apoptotic cell clearance by macrophages (efferocytosis) promotes resolution signaling pathways, which can be triggered by molecules derived from the phagolysosomal degradation of apoptotic cells. We show here that nucleotides derived from the hydrolysis of apoptotic cell DNA by phagolysosomal DNase2a activate a DNA–PKcs–mTORC2/Rictor pathway that increases Myc to promote non-inflammatory macrophage proliferation. Efferocytosis-induced proliferation expands the pool of resolving macrophages *in vitro* and in mice, including zymosan-induced peritonitis, dexamethasone-induced thymocyte apoptosis, and atherosclerosis regression. In the dexamethasone-thymus model, hematopoietic Rictor deletion blocked efferocytosing macrophage proliferation, apoptotic cell clearance, and tissue resolution. In atherosclerosis regression, silencing macrophage Rictor or DNase2a blocked efferocyte proliferation, apoptotic cell clearance, and plaque stabilization. In view of previous work showing that other types of apoptotic cell cargo can promote resolution in individual efferocytosing macrophages, the findings here suggest that signaling-triggered apoptotic cell-derived nucleotides can amplify this benefit by increasing the number of these macrophages.

INTRODUCTION

Macrophages play critical roles in tissue remodeling in normal physiology and in resolution of inflammation and tissue injury (Wynn et al., 2013). A critical process in resolution is the clearance of apoptotic cells (ACs), or efferocytosis (Boada-Romero et al., 2020; Dalli and Serhan, 2017; Doran et al., 2020; Henson, 2017; Morioka et al., 2019). Efferocytosis prevents tissue necrosis and inflammation by preventing necrosis of dead cells, and ACs activate receptor-mediated signaling pathways in macrophages that suppress inflammation and promote resolution and repair (Boada-Romero et al., 2020; Bosurgi et al., 2017; Cai et al., 2016; Camenisch et al., 1999; Dalli and Serhan, 2017; Doran et al., 2020; Henson, 2017; Lemke and Rothlin, 2008; McDonald et al., 1999; Morioka et al., 2019; Tibrewal et al., 2008). Macrophages are capable of high-capacity efferocytosis, which plays a critical role in the resolution process. For example, in hypercholesterolemic humans and mice with established atherosclerosis, marked lowering of plasma cholesterol triggers a burst of efferocytosis that mediates resolution and plaque stabilization, which lowers the risk of coronary artery disease in humans (Fisher, 2016; Sharma et al., 2020; Sipahi et al., 2006; Yurdagul et al., 2020). Conversely, efferocytosis becomes defective in many chronic inflammatory diseases, including progressing atherosclerosis, leading to tissue damage and chronic inflammation (Boada-Romero et al., 2020; Dalli and Serhan, 2017; Doran et al., 2020; Henson, 2017; Morioka et al., 2019). The pro-resolving/repair function of macrophages is influenced by specific intracellular metabolic pathways (O'Neill and Pearce, 2016). Some of these pro-resolving pathways are triggered by metabolites (e.g., amino acids and lipids) obtained from the phagolysosomal degradation of ACs during efferocytosis (A-Gonzalez et al., 2009; Morioka et al., 2018; Yurdagul et al., 2020; Zhang et al., 2019).

In this study, we explored another class of AC-derived molecules, namely nucleic acids. We found that nucleotides derived from the phagolysosomal hydrolysis of AC-DNA during efferocytosis trigger a signaling pathway that promotes the proliferation of pro-resolving macrophages. In resolving settings *in vivo* (e.g., sterile peritonitis, dexamethasone-induced thymocyte

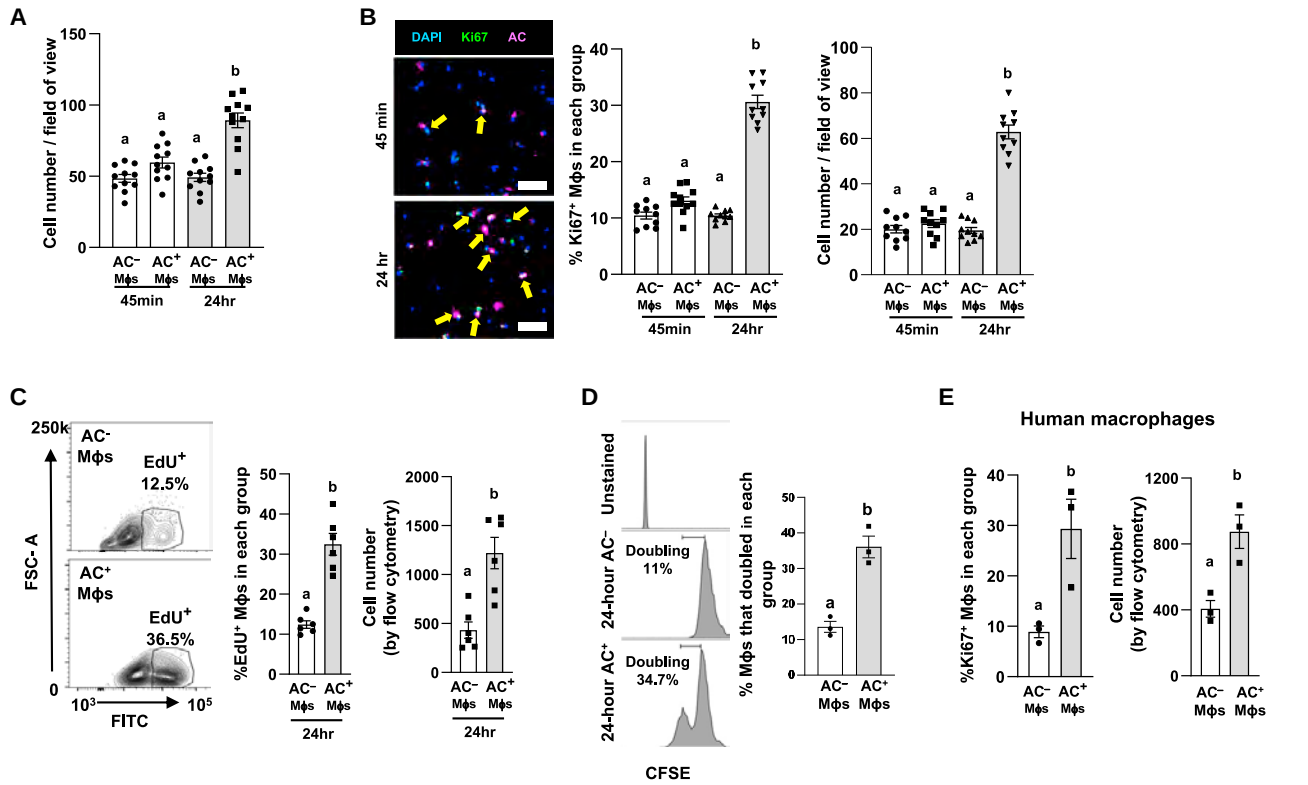

(legend on next page)

apoptosis, and atherosclerosis regression), efferocytic macrophages proliferate, and when the AC-oligonucleotide signaling pathway is inhibited, efferocytic macrophage proliferation is blocked and resolution is impaired.

RESULTS

Efferocytosing macrophages undergo proliferation

To study differences between efferocytosing and basal macrophages, we incubated bone marrow-derived macrophages (BMDMs) with Vybrant DiD-labeled apoptotic Jurkat cells for 45 min. The unengulfed ACs were then removed by rinsing, and the macrophages were either fixed immediately or incubated for an additional 24 h and then fixed. We use DiD-fluorescence to distinguish AC^+ from AC^- macrophages. At the 24-h time point, the number of AC^+ macrophages increased, whereas the number of AC^- macrophages did not change (Figure 1A). Further, ~30% of the AC^+ macrophage subpopulation, but not the AC^- subpopulation, displayed an increase in the percentage of macrophages expressing the proliferation marker $Ki67^+$ as well as the total number of macrophages (Figure 1B). We also used flow cytometry to analyze macrophages pre-incubated with 5-ethynyl-2′-deoxyuridine (EdU), a thymidine analog that is incorporated into newly synthesized DNA. Consistent with the above data, the percent of EdU^+ macrophages and total number of macrophages were higher in the AC^+ versus AC^- macrophage subpopulation at the 24-h time point (Figure 1C). As with Ki67, ~30% of AC^+ macrophages showed an increase in EdU positivity. As a final test, macrophages were pre-labeled with the cytoplasmic dye carboxyfluorescein diacetate succinimidyl ester (CFSE), a dye that is diluted in proliferating cells. Flow cytometric analysis showed a substantially higher level of CFSE dilution in AC^+ versus AC^- macrophages at the 24-h time point (Figure 1D), indicating that AC^+ macrophages undergo cell division. Similar results were obtained when we used apoptotic BMDMs (Figures S1A and S1B); when we gated on macrophages in which ACs were documented to be in phagolysosomes, i.e., by using ACs labeled with pHrodo dye, which requires an acidic environment for fluorescence emission (Figure S1C); or when we used human monocyte-derived macrophages (HMDMs) (Figures 1E and 1F).

The above experiments used BMDMs differentiated from monocytes in media that contained L-cell conditioned media but with no other treatment (basal macrophages). Another type of macrophage proliferation can be triggered by Th2 immunity, which can be modeled *in vitro* by treatment of basal macrophages with interleukin-4 (IL-4) (Bosurgi et al., 2017; Jarjour et al., 2019; Jenkins et al., 2011). We therefore questioned whether efferocytosis and IL-4 treatment might have additive effects on macrophage proliferation. As expected, each treatment alone increased macrophage proliferation, and we found that the combination of AC uptake and IL-4 treatment increased macrophage proliferation above that seen with either treatment alone (Figure S1D). In contrast, proliferation was very low in inflammatory macrophages generated by treatment with lipopolysaccharide (LPS) and interferon-γ (IFN-γ), and there was no response to efferocytosis (Figures S1E and S1F). In summary, efferocytosis triggers the proliferation of basal and resolving mouse and human macrophages, but not inflammatory macrophages. We call this process efferocytosis-induced macrophage proliferation (EIMP).

Proliferation of efferocytosing macrophages requires phagolysosomal degradation of ACs, with an additional stimulus from MerTK

To determine if phagolysosomal AC degradation was necessary for EIMP, we silenced Rubicon (siRbcn) (Figure S2A), a scaffold protein that is needed for a critical process in phagolysosomal

Figure 1. Efferocytosis induces macrophage proliferation

BMDMs were incubated with DiD-labeled apoptotic Jurkat cells (ACs) for 45 min, followed by rinsing to remove unengulfed ACs and then harvesting immediately or after an additional 24 h incubation in the absence of ACs unless otherwise specified.

(A) BMDMs from both time points were stained with DAPI, and cell number/field of view was assessed by counting DAPI-stained DiD^- (AC^-) and DiD^+ (AC^+) macrophages (n = 11 biological replicates).

(B) Left, fluorescence microscopic images of BMDMs harvested after 45 min (top) or 24 h (bottom). Yellow arrows identify DiD^+ (AC^+) $Ki67^+$ macrophages. Scale bar, 50 μm. Middle, percentage of $Ki67^+$ macrophages within the AC^- and AC^+ macrophage subpopulations. Right, AC^- and AC^+ macrophage numbers/field of view. For both analyses, n = 10 biological replicates.

(C) BMDMs were pre-labeled with EdU and then assayed by flow cytometry at the 24 h time point for the percentage of EdU^+ macrophages within the AC^- and AC^+ macrophages (left and middle) and for AC^- and AC^+ macrophage numbers (right) (n = 5 or 6 biological replicates).

(D) BMDMs were pre-labeled with CFSE for 15 min and then assayed by flow cytometry at the 24 h time point for the percentage of macrophages in each group that doubled, calculated from the decrease in CSFE fluorescence (n = 3 biological replicates).

(E) HMDMs were used instead of BMDMs and assayed by flow cytometry at the 24 h time point for the percentage of $Ki67^+$ cells within AC^- and AC^+ macrophages (left) and for AC^- and AC^+ macrophage numbers (right) (n = 3 biological replicates).

(F) HMDMs were incubated for 45 min in the absence or presence of ACs and assayed for the number of cells/well; dotted line indicates cell number at the beginning of the experiment (n = 3 biological replicates).

(G) BMDMs transfected with siRbcn or scrambled RNA control and labeled with EdU were harvested after the 24 h time point or at 48 h after removal of the labeled ACs and then assayed for the percentage of EdU^+ macrophages (n = 3 biological replicates).

(H) BMDMs transfected with siRbcn or scrambled RNA were incubated in the absence or presence of unlabeled ACs and quantified for cell number/well; dotted line indicates cell number at the beginning of the experiment (n = 3 biological replicates).

(I) Groups 1–4, BMDMs pre-treated with bafilomycin and labeled with EdU were harvested 18 h after labeled-AC removal and assayed for the percentage of EdU^+ macrophages. Groups 5–8, BMDMs were incubated with CSF1 or Gas6 for 18 h instead of ACs and assayed as above (n = 3 biological replicates).

(J) BMDMs from $Mertk^{fl/fl}$ or $Mertk^{fl/fl}Lyz2Cre^{+/-}$ mice labeled with EdU were harvested at 24 or 48 h time points and assayed for the percentage of EdU^+ macrophages.(n = 3 biological replicates)

(K) BMDMs from $Mertk^{fl/fl}$ or $Mertk^{fl/fl}Lyz2Cre^{+/-}$ mice pre-treated with bafilomycin and labeled with EdU were harvested at 24 or 48 h time points and assayed for the percentage of EdU^+ macrophages (n = 3 biological replicates).

All values are means ± SEM; letters that are different indicate statistical significance at $p < 0.05$.

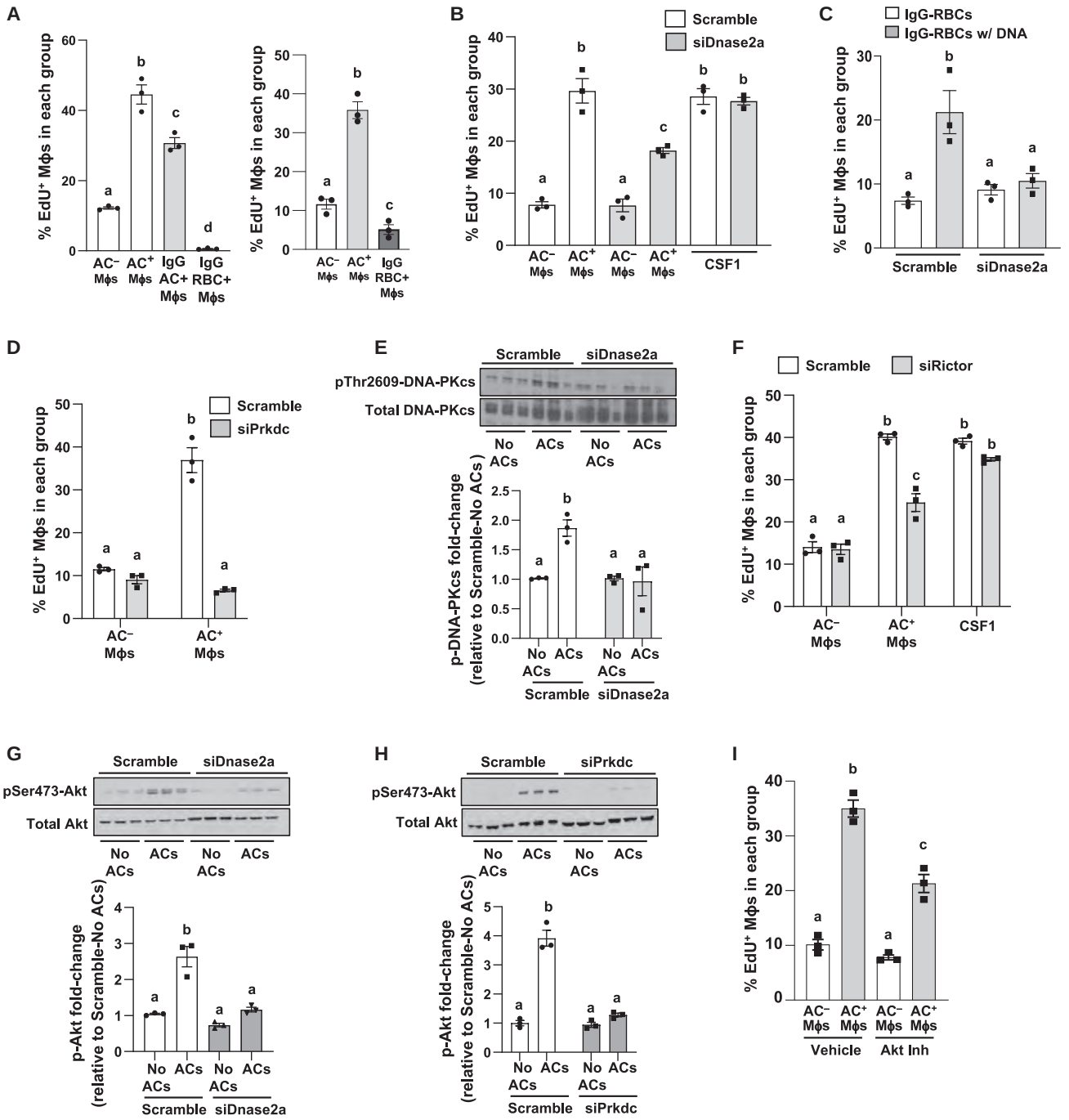

Figure 2. Degradation of AC-derived oligonucleotides activate DNA-PKcs and mTORC2 activity to promote EIMP

The standard conditions are as in Figure 1 unless noted otherwise.

(A) BMDMs were incubated for 45 min with DiD-labeled (left) or pHrodo-labeled (right) ACs, IgG-coated ACs, or IgG-coated RBCs. At the 24 h time point, the macrophages were quantified by flow cytometry for the percentage of EdU$^+$ macrophages (n = 3 biological replicates).

(B) Groups 1–4, BMDMs transfected with siDNase2a or scrambled RNA and labeled with EdU were assayed at the 24 h time point for the percentage of EdU$^+$ macrophages. Groups 5 and 6, BMDMs were incubated with CSF1 for 24 h instead of ACs and assayed as above (n = 3 biological replicates).

(C) BMDMs transfected with siDNase2a or scrambled RNA and labeled with EdU were incubated with IgG-RBCs or IgG-RBCs containing salmon sperm DNA and assayed at the 24 h time point for the percentage of EdU$^+$ macrophages (n = 3 biological replicates).

(D) BMDMs transfected with siPrkdc or scrambled RNA and labeled with EdU were assayed at the 24 h time point for the percentage of EdU$^+$ macrophages (n = 3 biological replicates).

(E) BMDMs transfected with siDNase2a or scrambled RNA were incubated for 1 h in the absence or presence of ACs. Lysates were immunoblotted for phospho-Thr2609-DNA-PKcs and total DNA-PKc; the graph shows the phospho:total DNA-PKcs densitometric ratio, expressed relative to no ACs/scramble control (n = 3 biological replicates).

(legend continued on next page)

function during efferocytosis called LC3-associated phagocytosis (Martinez et al., 2015). Scrambled RNA- and siRbcn-treated BMDMs were pulsed with EdU and incubated with DiD-labeled ACs for 45 min and assayed for the percentage of EdU^+ macrophages at 24 or 48 h after AC removal, as above. Rubicon silencing, despite not blocking of the initial uptake of ACs (Figure S2B, left), resulted in a marked decrease in the percent of EdU-positivity in AC^+ macrophages at both time points (Figure 1G). Moreover, the increment in cell number after incubation with ACs was suppressed by Rubicon silencing (Figure 1H). Bafilomycin, which inhibits phagolysosomal acidification and degradation of internalized ACs (Bagaitkar et al., 2018; Yurdagul et al., 2020), also blocked the percent of EdU-positivity in AC^+ macrophages (Figure 1I, bars 1–4) despite no effect on initial AC uptake **(**Figure S2B, right**)**. As an important control, we showed that colony-stimulating factor-1 (CSF1)-induced macrophage proliferation, which should not involve phagolysosomes, was not blocked by bafilomycin (Figure 1I, bars 5 and 6).

Although blocking phagolysosomal degradation of ACs markedly suppressed EIMP, there was a residual AC-induced proliferative response (Figure 1I, bars 3 and 4). To explain this finding, we hypothesized that the initial activation of a signaling receptor by ACs may contribute partially to EIMP, focusing on the efferocytosis receptor MerTK (Lemke and Rothlin, 2008). BMDMs derived from $MerTK^{fl/fl}$ (control) or $MerTK^{fl/fl}Lyz2Cre^{+/-}$ (myeloid-MerTK-deleted) mice (Cai et al., 2020; Fourgeaud et al., 2016) were exposed to DiD-labeled ACs and then assayed for the percent of EdU^+ macrophages at 24 and 48 h. Note that although efferocytosis is ~50% inhibited in macrophages lacking MerTK (Figure S2C), the analysis focused on the subset of macrophages that internalized DiD-ACs despite the absence of MerTK. We found that the percent of EdU^+ cells was lower in AC^+ macrophages lacking MerTK as compared with control AC^+ macrophages (Figure 1J). Further, the increase in macrophage number induced by ACs was also lower in macrophages lacking MerTK (Figure S2D). In contrast, Axl-lacking macrophages, which have a smaller defect in efferocytosis than $Mertk^{-/-}$ macrophages (Subramanian et al., 2016), showed no defect in the percent of EdU^+ cells in AC^+ macrophages or in the increase in cell number induced by ACs (Figures S2E and S2F, bars 7 and 8). Likewise, silencing the efferocytosis receptor CD36 (Xiong et al., 2013) had no effect on EIMP **(**Figure S2G). We also showed that macrophage proliferation induced by CSF1 was not decreased by MerTK deletion (or by Axl knockout) (Figures S2E and S2F, bars 9–11), which further distinguishes EIMP from CSF1-induced macrophage proliferation.

To further distinguish the MerTK and phagolysosomal pathways in EIMP, we showed that the MerTK ligand Gas6 promoted a modest level of macrophage proliferation, and, as predicted, it was not significantly blocked by bafilomycin (Figure 1I, bars 7 and 8). Further, we found that the combination of bafilomycin treatment and MerTK absence markedly abrogated the percent increase in EdU-positivity in AC^+ macrophages compared with either perturbation alone (Figure 1K). Thus, two separate pathways contribute to EIMP: a pathway requiring degradation of ACs in phagolysosomes and a pathway downstream of MerTK, which likely becomes activated by AC-bound Gas6 prior to AC engulfment.

EIMP requires the phagolysosomal release of AC-derived oligonucleotides, which activate mTORC2 through DNA-PKcs

Given that cell cycling is the biological endpoint of EIMP, we considered that nucleotides derived from the hydrolysis of AC-DNA might be the key trigger of the phagolysosomal branch of EIMP. As an initial test of this idea, we incubated macrophages with DiD-labeled immunoglobin G (IgG)-coated red blood cells (IgG-RBCs), which lack DNA, versus ACs or DiD-labeled IgG-coated ACs (IgG-ACs). Consistent with our previous results, macrophages that had ingested DiD-labeled ACs were enriched for EdU labeling, which was also observed in macrophages that had ingested DiD-labeled IgG-ACs (Figure 2A, left, bars 1–3). However, the macrophages that ingested IgG-RBCs did not show this response even though the uptake was similar to that of ACs (Figures 2A [left, bar 4] and S3A). To correct for differences in AC- versus IgG-RBC internalization into phagolysosomes, we used pHrodo-labeled ACs and pHrodo-labeled RBCs and gated on macrophages with similar fluorescence, which confirmed that macrophages with internalized RBCs do not undergo proliferation (Figure 2A, right graph). These findings are consistent with the notion that AC-DNA is important for the EIMP response.

To test causation, we assayed EIMP in macrophages with silenced DNase2a (Figure S3B), the phagolysosomal enzyme that digests AC-DNA into oligonucleotides (Minchew and Didenko, 2011). Silencing DNase2a resulted in decreased EdU incorporation into AC^+ macrophages and less AC-induced increase in cell number compared with macrophages transfected with scrambled RNA (Figures 2B [bars 1–4] and S3C). Note that siDNase2a did not block the initial uptake of ACs (Figure S3D) and did not trigger autophagy (Lan et al., 2014) based on the lack of an increase in punctate LC3-II staining (Figure S3E). Moreover, exogenous addition of nucleotide triphosphates did not rescue the proliferation defect observed in DNase2a-silenced macrophages **(**Figure S3F**)**. As with siRbcn and bafilomycin, DNase2a silencing had no effect on CSF1-induced EdU incorporation (Figure 2B, bars 5 and 6). Moreover, neither silencing of DNase1 (Figure S3G, left), a cytosolic enzyme that

(F) Pair groups 1 and 2, BMDMs transfected with siRictor or scrambled RNA and labeled with EdU were assayed at the 24 h time point for the percentage of EdU^+ macrophages. Pair group 3, BMDMs were incubated with CSF1 for 24 h instead of ACs and assayed as above (n = 3 biological replicates).
(G) BMDMs transfected with scrambled RNA or siDNase2a were incubated for 1 h in the absence or presence of ACs. Lysates were immunoblotted for phospho-Ser473-Akt and total Akt, with quantification (n = 3 biological replicates).
(H) BMDMs transfected with scrambled RNA or siPrkdc were incubated for 1 h in the absence or presence of ACs. Lysates were immunoblotted for phospho-Ser473-Akt and total Akt, with quantification (n = 3 biological replicates).
(I) BMDMs treated with vehicle or the Akt inhibitor MK-2206 for 2 h and labeled with EdU were assayed at the 24 h time point for the percentage of EdU^+ macrophages (n = 3 biological replicates).
All values are means ± SEM; letters that are different indicate statistical significance at $p < 0.05$.

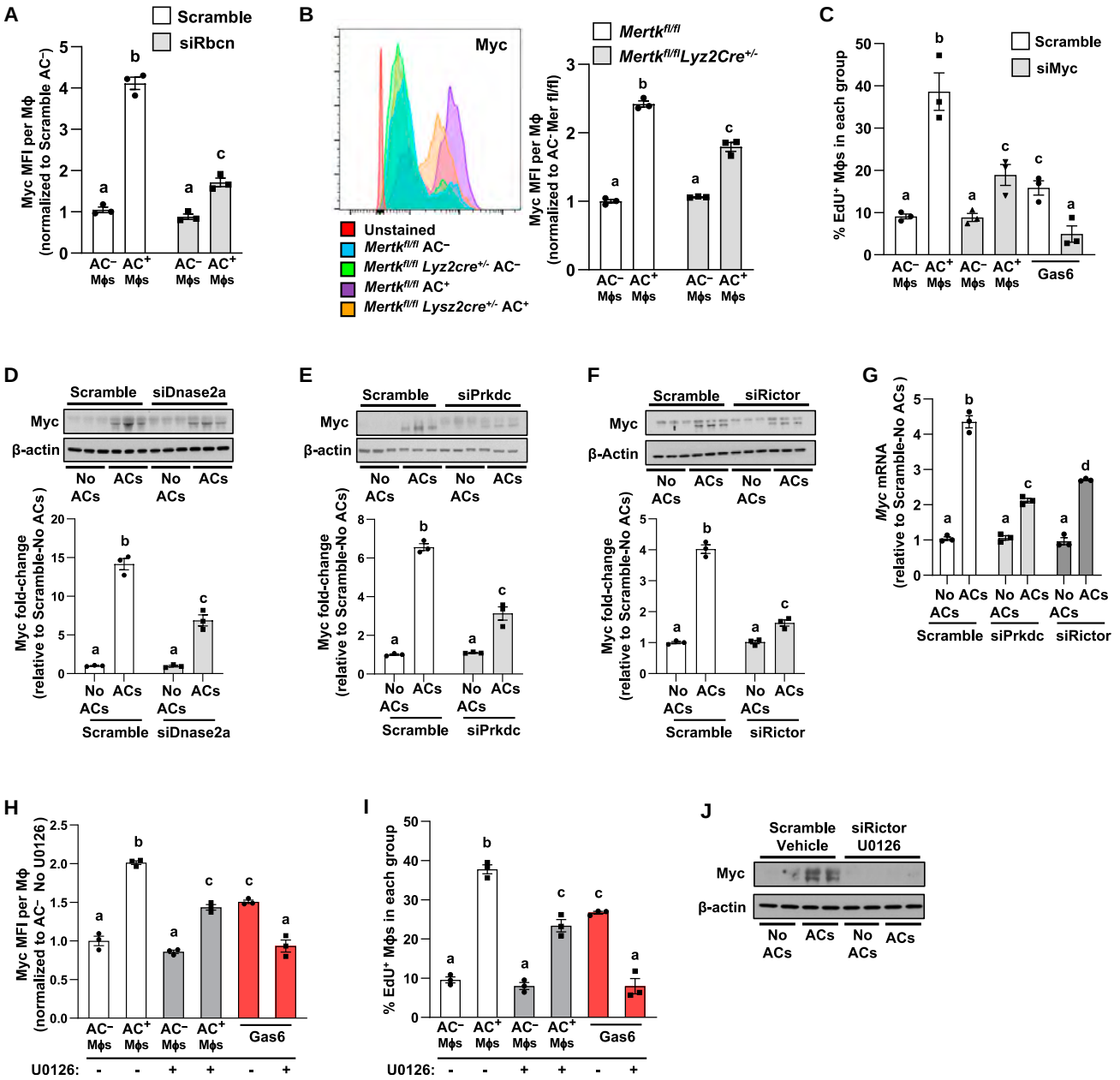

Figure 3. Mertk-ERK1/2 and mTORC2 are both necessary for full Myc expression during EIMP

The standard conditions are as in Figure 1 unless noted otherwise.

(A) BMDMs transfected with scrambled RNA or siRbcn were harvested 3 h after removal of the labeled ACs, immunostained for intracellular Myc, and assayed for Myc MFI, gating on AC^- and AC^+ macrophages (n = 3 biological replicates).

(B) BMDMs from *Mertk*$^{fl/fl}$ or *Mertk*$^{fl/fl}$ *Lyz2Cre*$^{+/-}$ mice were harvested 3 h after removal of the labeled ACs, immunostained for intracellular Myc, and assayed for Myc MFI, gating on AC^- and AC^+ macrophages (n = 3 biological replicates).

(C) Groups 1–4, BMDMs transfected with siMyc or scrambled RNA and labeled with EdU were assayed at the 24 h time point for the percentage of EdU^+ macrophages. Groups 5 and 6, BMDMs were incubated with Gas6 for 24 h instead of ACs and assayed as above (n = 3 biological replicates).

(D–F) BMDMs transfected with scrambled RNA, siDNase2a, siPrkdc, or siRictor were incubated in the absence or presence of ACs for 45 min and harvested 3 h later. Lysates were immunoblotted for Myc and β-actin; the graph shows the Myc:β-actin densitometric ratio, expressed relative to no ACs/scramble control (n = 3 biological replicates).

(G) BMDMs transfected with scrambled RNA, siDNase2a, siPrkdc, or siRictor were incubated in the absence or presence of ACs for 45 min, harvested 3 h later, and assayed for *Myc* mRNA (n = 3 biological replicates).

(H) Groups 1–4, BMDMs treated ± U0126 were harvested at the 3 h time point and assayed for Myc in AC^- and AC^+ macrophages by flow cytometry. Groups 5 and 6, BMDMs were incubated with Gas6 instead of ACs and assayed as above (n = 3 biological replicates).

(legend continued on next page)

degrades DNA into nucleotides, nor silencing of glucose-6-phosphate-dehydrogenase (G6pdx) (Figure S3G, right), a rate-limiting enzyme involved in the pentose phosphate pathway that produces *de novo* nucleotides, blocked EIMP (Figure S3H). Finally, we revisited the IgG-RBC system, this time electroporating salmon sperm DNA into the RBCs. The DNA-loaded IgG-RBCs were able to stimulate macrophage EdU incorporation as compared with unloaded IgG-RBCs, and this proliferative response was blunted in macrophages treated with siDNase2a (Figure 2C). Together, these results show that AC-derived oligonucleotides generated by phagolysosomal DNase2a is necessary for EIMP.

To uncover the mechanistic link between DNase2a-derived oligonucleotides and EIMP, we searched for enzymes that are capable of binding DNA oligonucleotides and associated with proliferation and considered DNA-dependent protein kinase (DNA-PK). DNA-PK, which consists of a catalytic subunit called DNA-PKcs (gene name *Prkdc*) and a nucleotide-binding domain (Dynan and Yoo, 1998), can promote cell proliferation by activating mTORC2 (Zheng et al., 2016). To test the involvement of DNA-PKcs in EIMP, we treated BMDMs with siPrkdc or scrambled RNA (Figure S3I) and conducted an EdU-incorporation assay. We found that siPrkdc, which had no effect on initial AC uptake (Figure S3J), markedly inhibited the percent of EdU$^+$ macrophages within the AC$^+$ subpopulation (Figure 2D). Further, phosphorylation of DNA-PKcs, which is a marker of activation, was increased in AC$^+$ versus AC$^-$ macrophages, and this increase was completely abrogated by siDNase2a (Figure 2E). Thus, phagolysosomal degradation of AC-DNA activates DNA-PKcs, which is necessary for EIMP.

We questioned whether AC-derived nucleotides, in addition to activating DNA-PKcs, might also be incorporated into the nuclei of macrophages undergoing EIMP. We first incubated Jurkat cells with EdU for 2 h such that a portion of the cells, i.e., those undergoing DNA synthesis during this period, would have their DNA labeled. The Jurkat cells were then rendered apoptotic, labeled with DiD, and added to control (scrambled RNA-treated), siDNase2a-treated, and bafilomycin-treated macrophages for 45 min. The non-internalized ACs were then rinsed away, and the macrophages were incubated for an additional 18 h. We found that ~40% of the nuclei of control macrophages showed EdU staining that could not be explained by EdU in residual DiD$^+$ AC material (Figure S3K). With siDNase2a treatment, most of the EdU label was associated with residual DiD$^+$ AC material, with much less incorporated into macrophage nuclei. As expected, bafilomycin-treated macrophages showed the presence of undegraded DiD$^+$ EdU$^+$ ACs, with very little EdU label in macrophage nuclei. These data are consistent with the idea that macrophages undergoing EIMP use nucleotides derived from hydrolysis of AC-DNA to synthesize DNA.

We next further explored the DNA-PKcs-mediated signaling role of AC nucleotides in EIMP. In view of the aforementioned mTORC2 link (Zheng et al., 2016) and previous data showing that platelet-derived growth factor-induced macrophage proliferation is impaired in macrophages lacking the key mTORC2 protein Rictor (Babaev et al., 2018), we tested the role of mTORC2 in EIMP by silencing Rictor. Treatment of macrophages with siRictor (Figure S3L), which does not block initial AC uptake (Figure S3M), decreased the percent of EdU$^+$ macrophages within the AC$^+$ subpopulation but had no effect on CSF1-induced EdU incorporation (Figure 2F). Further, ACs induced phosphorylation of Akt at serine-473 (Figures 2G and 2H), which is an mTORC2-mediated process necessary for proliferation in another setting (Zheng et al., 2016), and this was prevented by both siDNase2a and siPrkdc. Additionally, inhibiting Akt with the pan-Akt inhibitor MK-2206 (Yoshida et al., 2015) inhibited EIMP (Figure 2I). These combined data support a role for the following pathway in EIMP: DNase2a-hydrolyzed AC-DNA → DNA-PKcs → mTORC2 → phospho-Akt → proliferation.

Increased Myc expression downstream of both mTORC2 and MerTK-ERK1/2 signaling is necessary for EIMP

In this section, we present evidence that both the MerTK and phagolysosomal-nucleotide pathways converge on the pro-proliferative transcription factor Myc (Carroll et al., 2018) to promote EIMP. To begin, we found that AC$^+$ macrophages had a higher level of Myc than AC$^-$ macrophages and that this increase was blunted by siRbcn and in *Mertk*$^{-/-}$macrophages (Figures 3A, 3B, and S3N). Most importantly, the percentage of EdU$^+$ cells within both AC$^+$ macrophages and Gas6-treated macrophages was suppressed by silencing Myc (Figures 3C and S3O) despite no change in initial AC uptake (Figure S3P). Thus, both the phagolysosomal degradation of ACs and the engagement of MerTK increases Myc expression to stimulate EIMP.

With regard to the phagolysosomal pathway, we asked whether the aforementioned DNase2a-DNA-PKcs-mTORC2 pathway might contribute to increased Myc. Indeed, the silencing of DNase2a, DNA-PKcs, or Rictor led to decreases in both Myc protein and *Myc* mRNA (Figures 3D–3G). With regard to MerTK, we postulated that activation of ERK1/2 might be involved, as MerTK engagement leads to ERK1/2 activation, including in macrophages (Cai et al., 2018; Nishi et al., 2019; Schlegel et al., 2013), and ERK1/2 has been linked to increased Myc expression in other cell types (Sears et al., 1999). As expected, AC$^+$ macrophages had increased phospho-ERK1/2, a measure of ERK1/2 activation, when compared with AC$^-$ macrophages, and phospho-ERK1/2 was decreased in AC$^+$ macrophages lacking MerTK (Figure S3Q). To test causation in EIMP, macrophages were pre-treated with U0126, a MEK inhibitor that prevents Erk1/2 phosphorylation (Favata et al., 1998), and then incubated with EdU and either DiD-labeled ACs or Gas6. The ERK inhibitor suppressed Myc expression (Figures 3H and S3R) and decreased the percentage of EdU$^+$ cells within both AC$^+$ macrophages and Gas6-treated macrophages (Figure 3I). Finally, when both the mTORC2 and ERK pathways were inhibited by siRictor and U0126, AC-induced Myc was almost

(I) Groups 1–4, BMDMs treated ± U0126 and labeled with EdU were harvested at the 24 h time point and assayed for the percentage of EdU$^+$ macrophages. Groups 5 and 6, BMDMs were incubated with Gas6 instead of ACs and assayed as above (n = 3 biological replicates).
(J) BMDMs transfected with scrambled RNA or siRictor were treated ± U0126 and then incubated in the absence or presence of ACs for 45 min, harvested at the 3 h time point, and immunoblotted for Myc and β-actin.
All values are means ± SEM; letters that are different indicate statistical significance at $p < 0.05$.

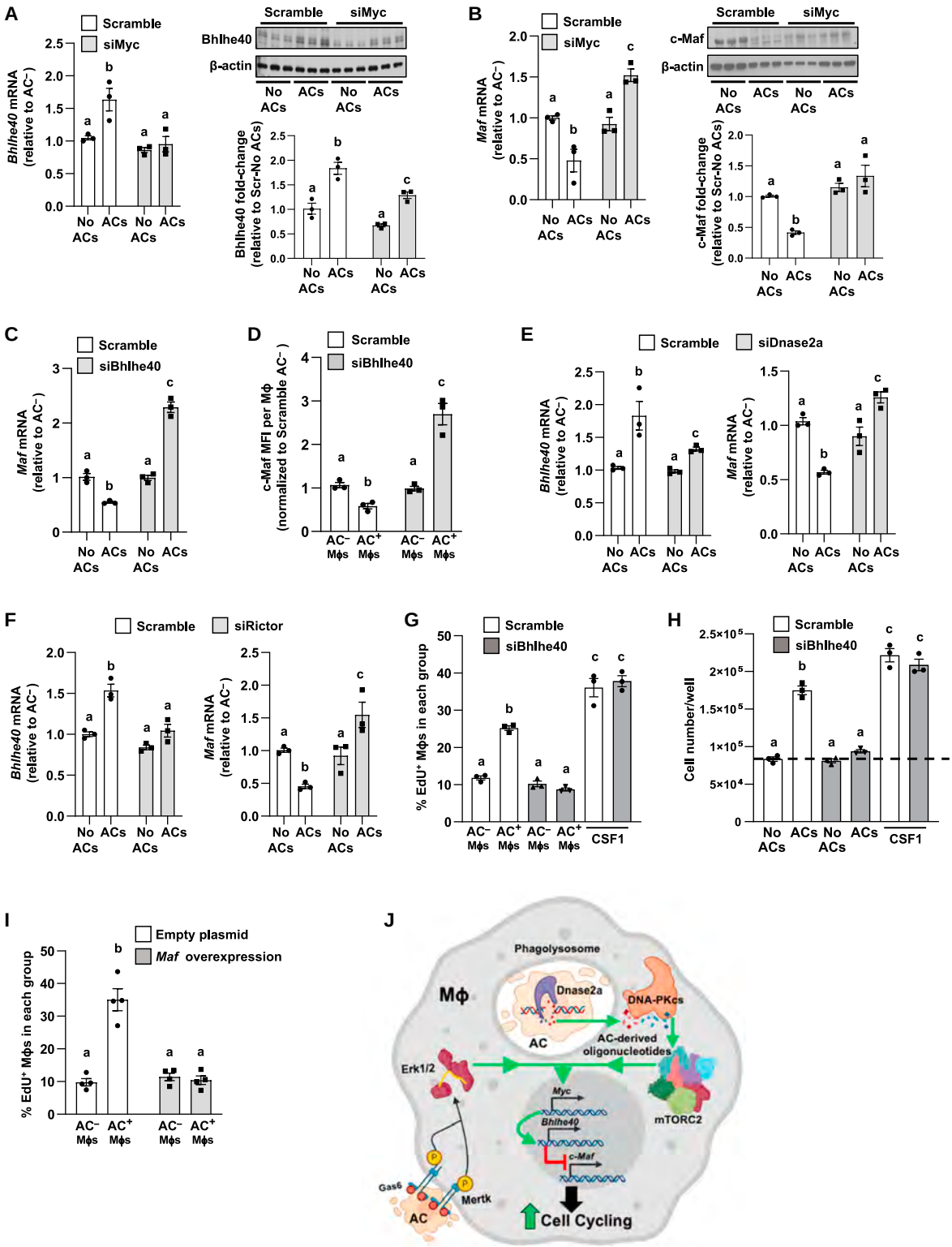

Figure 4. Myc drives EIMP by upregulating Bhlhe40 and downregulating c-Maf

The standard conditions and n number are as in Figure 1 unless noted otherwise.

(A) BMDMs transfected with scrambled RNA or siMyc were incubated in the absence or presence of ACs for 45 min, harvested 6 h later, and assayed for *Bhlhe40* mRNA (left) or Bhlhe40 protein by immunoblot (right). The graph shows the Bhlhe40:β-actin densitometric ratio, expressed relative to no ACs/scramble control (n = 3 biological replicates).

(legend continued on next page)

completely suppressed (Figure 3J). Thus, the phagolysosomal and MerTK pathways, via mTORC2 and ERK1/2, respectively, combine to increase Myc in efferocytosing macrophages, which is necessary for EIMP.

Myc drives EIMP by upregulating Bhlhe40 and downregulating c-Maf

In a different setting of macrophage proliferation, the Myc target Bhlhe40 was shown to increase macrophage proliferation by downregulating the anti-proliferative protein c-Maf (gene name *Maf*) (Jarjour et al., 2019; Rauschmeier et al., 2019). We therefore asked whether Myc might drive EIMP by increasing the expression of Bhlhe40. Incubating macrophages with ACs increased *Bhlhe40* mRNA and Bhlhe40 protein, and Myc silencing blunted these increases (Figure 4A). Further, incubating macrophages with ACs decreased *Maf* mRNA and c-Maf protein, and Myc silencing prevented these decreases (Figures 4B and S4A). We established a link between Bhlhe40 and c-Maf by showing that silencing Bhlhe40 (Figure S4B) prevented the AC-induced decrease in *Maf* mRNA and c-Maf protein (Figures 4C and 4D) without blocking initial AC uptake (Figure S4C). Further, silencing either DNase2a or Rictor prevented the AC-induced increase in Bhlhe40 and decrease in c-Maf (Figures 4E, 4F, and S4D). Most importantly, silencing Bhlhe40 completely prevented the increase in EdU incorporation in AC^+ macrophages and the increase in cell number in macrophages incubated with ACs, which was not seen with CSF1-induced proliferation (Figures 4G and 4H). Finally, transfection of macrophages with c-Maf (Figure S4E) blocked the increase in EdU incorporation into AC^+ macrophages (Figure 4I). In summary, AC-mediated activation of MerTK-ERK signaling together with activation of DNA-PKcs-mTORC2 signaling by DNase2a-derived AC-oligonucleotides induces *Myc* to a high enough level where it induces *Bhlhe40*. Bhlhe40 then represses the cell-cycling-inhibitor c-Maf to drive proliferation (Figure 4J).

Macrophages undergoing EIMP are competent efferocytes and producers of TGFβ and IL-10 *in vitro*

We reasoned that EIMP would expand the pool of macrophages capable of clearing ACs and producing pro-resolving molecules. We therefore tested whether macrophages that had undergone EIMP were adequate at carrying out efferocytosis and producing two efferocytosis-induced resolving/repair proteins, transforming growth factor-β (TGFβ) and interleukin-10 (IL-10) (Fadok et al., 1998; Voll et al., 1997). We generated AC-induced proliferating macrophages by incubating BMDMs with unlabeled ACs for 45 min, followed by a 24 h incubation. Proliferating macrophages were identified by Ki67-positivity, and a majority of these $Ki67^+$ macrophages were undergoing efferocytosis, i.e., had internalized an AC. We then compared these "EIMP macrophages" with control non-EIMP macrophages, i.e., $Ki67^-$ macrophages that did not undergo an initial incubation with unlabeled ACs, for their relative abilities to carry out efferocytosis and post-efferocytic TGFβ and IL-10 production.

For efferocytosis, we assayed both single AC uptake as well as the key resolving process of continual efferocytosis (Park et al., 2011; Wang et al., 2017; Yurdagul et al., 2020). To assay single-AC efferocytosis, the two groups of macrophages were incubated with PKH67-labeled ACs for 45 min, followed by AC removal and quantification of PKH67 uptake. For continual efferocytosis, control and EIMP macrophages were first incubated as above with PKH67-labeled ACs, followed by rinsing and a 2 h incubation in medium alone. The macrophages were then incubated for 45 min with PKH26-labeled ACs and quantified for PKH67 and PKH26 double-positivity among all $PKH67^+$ macrophages (Yurdagul et al., 2020). The data show that EIMP macrophages ingested single PKH67-labeled ACs to the same extent as control macrophages, and they showed an even greater ability to engulf a second AC (Figures 5A and 5B).

To assess TGFβ and IL-10 production, macrophages were pre-incubated with EdU and then incubated with DiD-labeled ACs for 45 min and then, after removal of unengulfed ACs, cultured for an additional 18 h. Golgi-stop was added to the cells at the beginning of the 18 h incubation to enable quantification of intracellular TGFβ and IL-10. AC^+ and AC^- macrophages were then assayed for intracellular TGFβ and IL-10 by flow cytometry. As expected (Fadok et al., 1998; Voll et al., 1997), TGFβ and IL-10 were higher in AC^+ versus AC^- macrophages in the non-EIMP (EdU^-) control cohort. Most importantly, the AC-induced increments in TGFβ and IL-10 were also seen in EIMP (EdU^+) macrophages (Figures 5C, 5D, S4F, and S4G). In summary, macrophages undergoing EIMP are highly competent at both efferocytosis and efferocytosis-induced production of two key pro-resolving cytokines.

(B) BMDMs transfected with scrambled RNA or siMyc were incubated in the absence or presence of ACs for 45 min, harvested 6 h later, and assayed for *Maf* mRNA (left) or c-Maf protein by immunoblot, with quantification (right) (n = 3 biological replicates).
(C) BMDMs transfected with scrambled RNA or siBhlhe40 were incubated in the absence or presence of ACs for 45 min, harvested 6 h later, and assayed for *Maf* mRNA (n = 3 biological replicates).
(D) BMDMs transfected with scrambled RNA or siBhlhe40 were harvested at the 6 h time point and assayed for c-Maf in AC^- and AC^+ macrophages by flow cytometry (n = 3 biological replicates).
(E and F) BMDMs transfected with scrambled RNA, siDNase2a, or siRictor, and incubated in the absence or presence of ACs were assayed at the 6 h time point for *Bhlhe40* and *Maf* mRNA (n = 3 biological replicates).
(G) Groups 1–4, BMDMs transfected with scrambled RNA or siBhlhe40 and then labeled with EdU were harvested at the 24 h time point and assayed for the percentage of EdU^+ macrophages. Groups 5 and 6, BMDMs were incubated for 24 h with CSF1 instead of ACs and assayed as above (n = 3 biological replicates).
(H) Groups 1–4, BMDMs transfected with scrambled RNA or siBhlhe40 were incubated in the absence or presence of ACs and assayed at the 24 h time point for cell number/well. Groups 5 and 6, BMDMs were incubated for 24 h with CSF1 instead of ACs and assayed as above (n = 3 biological replicates).
(I) BMDMs transfected with empty plasmid or *Maf*-encoding plasmid and then labeled with EdU were harvested at the 24 h time point and assayed for the percentage of EdU^+ macrophages (n = 3 biological replicates).
(J) Schematic summary of the EIMP pathway. AC-mediated activation of MerTK-ERK signaling and activation of DNA-PKcs-mTORC2 signaling by DNase2a-derived AC-oligonucleotides converge to induce *Myc*, which then induces *Bhlhe40*. Bhlhe40 represses the cell-cycling-inhibitor c-Maf to drive macrophage proliferation.
All values are means ± SEM; letters that are different indicate statistical significance at $p < 0.05$.

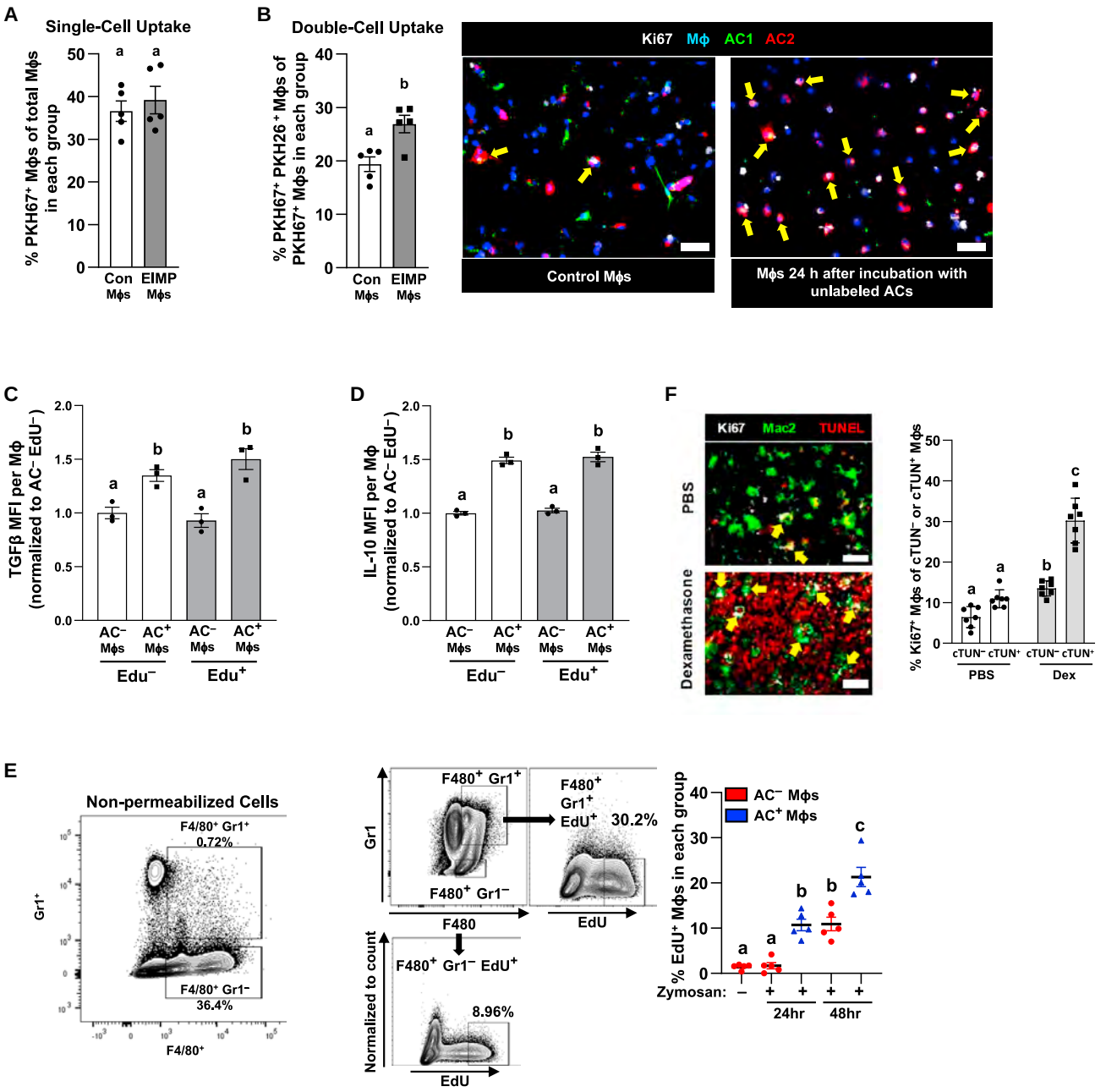

Figure 5. Macrophages undergoing EIMP are competent efferocytes and producers of TGFβ and IL-10 *in vitro*, and evidence of EIMP *in vivo*

(A) Macrophages not previously exposed to ACs and shown to be Ki67$^-$ (control Mφs) or Ki67$^+$ macrophages after 24 h incubation with unlabeled ACs (AC-induced proliferating macrophages, termed "EIMP Mφs") were incubated with PKH67-labeled ACs for 45 min. The percentage of PKH67$^+$ macrophages of total macrophages was assayed as a measure of single-cell efferocytosis (n = 5 biological replicates).

(B) Control and Ki67$^+$ EIMP macrophages were incubated with PKH67-labeled ACs for 45 min. After AC removal and rinsing, the macrophages were incubated for 2 h and then incubated with PKH26-labeled ACs for 45 min. The percentage of PKH67$^+$ PKH26$^+$ macrophages of PKH67$^+$ macrophages for each group was assayed as a measure of double-cell (continual) efferocytosis (n = 5 biological replicates). Right, representative fluorescence microscopic images for this experiment. Yellow arrows indicate PKH67$^+$ PKH26$^+$ Ki67$^+$ macrophages. Scale bar, 50 μm.

(C and D) EdU-labeled macrophages were incubated with DiD-labeled ACs for 45 min, rinsed, and incubated an additional 18 h. The cells were detached, immunostained for intracellular TGFβ and IL-10, and subjected to flow cytometric analysis to assess TGFβ and IL-10 mean fluorescence intensity (n = 3 biological replicates). Golgi-stop was added to the cells at the beginning of the 18 h incubation to enable quantification of intracellular TGFβ and IL-10.

(E) Mice were injected with EdU (200 μg/mouse i.p.) 24 h prior to injection with PBS or 1 mg of zymosan A. After 24 or 48 h, peritoneal cells were immunostained for F4/80 and intracellular Gr1 and subjected to flow cytometric analysis. Left, flow cytometry plot showing that macrophage permeabilization is needed to detect

(legend continued on next page)

EIMP occurs *in vivo* in acute models of high-burden efferocytosis

As an initial inquiry into the presence of EIMP *in vivo*, we examined a model of sterile peritoneal inflammation in which the yeast cell wall component zymosan A is injected into the peritoneal cavity of mice. In this model, the inflammatory stimulus of zymosan leads to neutrophil recruitment, which peaks at 12 h, followed by neutrophil apoptosis and apoptotic neutrophil clearance by intraperitoneal resolving-type macrophages (Pashover-Schallinger et al., 2012; Proto et al., 2018). To assess macrophage proliferation, the mice were injected intraperitoneally (i.p.) with EdU 24 h prior to the injection of vehicle or zymosan. At 24 and 48 h after zymosan injection, peritoneal cells were harvested and immunostained for the cell-surface marker F4/80 to identify macrophages and for intracellular Gr1, a marker of neutrophils (Figure S4H). Flow cytometric analysis was then conducted to quantify the percent of EdU^+ macrophages within the $Gr1^+$ (AC^+) and $Gr1^-$ (AC^-) macrophage subpopulations. At both 24 and 48 h time points, the percentage of EdU^+ cells was higher in AC^+ versus AC^- macrophages (Figure 5E), consistent with EIMP in this setting.

We next turned to a well-characterized model of high-burden efferocytosis in which mice are injected with dexamethasone to induce robust thymocyte apoptosis (dex-mice). High-capacity, continual efferocytosis by thymic macrophages limits the accumulation of dead thymocytes, which protects against tissue necrosis and inflammation (Park et al., 2011; Yurdagul et al., 2020). Efferocytic macrophages are identified by staining thymic sections with anti-Mac2 to identify macrophages and with TUNEL reagent to mark engulfed dead thymocytes, i.e., macrophages with cytoplasmic TUNEL staining (Park et al., 2011; Yurdagul et al., 2020). Note that thymocytes with nuclear TUNEL (dead cells) are very rare in this model (Figure S5A). We assayed Ki67-staining to determine whether efferocytosing (AC^+) macrophages were more proliferative than non-efferocytosing (AC^-) macrophages in dex-mice versus phosphate buffer solution (PBS)-treated control mice. As expected, efferocytosing macrophages were uncommon in the thymi of PBS-treated control mice owing to the paucity of apoptotic thymocytes (Figure 5F, top), and the small AC^+ macrophage subpopulation was not significantly enriched in $Ki67^+$ macrophages compared with the AC^- macrophage subpopulation (Figure 5F, bars 1 and 2). As expected, AC^+ macrophages were readily observed in the dex-mice thymi (Figure 5F, bottom), and, most importantly, there was a higher percentage of $Ki67^+$ cells within AC^+ versus AC^- macrophages (Figure 5F, bars 3 and 4).

To determine the role of Rictor, we examined the dex-thymus model in mice transplanted with $Rictor^{fl/fl}$ bone marrow cells that were first incubated *in vitro* with vehicle (control) or with TAT-Cre to delete Rictor prior to transplantation. As designed, bone marrow cells subsequently harvested from the mice transplanted with $Rictor^{fl/fl}$ TAT-Cre cells had undetectable Rictor, as did the macrophages in the thymi of these mice (Figure S5B). We found that the percent of $Ki67^+$ cells within the AC^+ macrophage subpopulation and the total number of macrophages were much lower in the thymi of the $Rictor^{fl/fl}$ TAT-Cre mice versus control mice (Figures 6A and 6B), without a change in thymic macrophage death (Figure S5C).

As further evidence for EIMP in the dex-thymus model, we found that AC^+ thymic macrophages expressed a higher level of Myc compared with AC^- macrophages in control $Rictor^{fl/fl}$-transplanted dex-mice, but this increase was much less in dex-mice whose macrophages lacked Rictor (Figures 6C [left] and S5D [top]). Moreover, as predicted by the EIMP pathway, Bhlhe40 expression in thymic macrophages was increased in AC^+ macrophages of control dex-mice but not dex-mice whose macrophages lacked Rictor (Figures 6C [middle] and S5D [middle]). Further, although c-Maf expression showed only a slight trend toward lower expression of AC^+ versus AC^- thymic macrophages in control dex-mice mice, its expression was markedly increased in AC^+ thymic macrophages in Rictor-deficient dex-mice (Figures 6C [right]and S5D [bottom]). Thus, suppression of EIMP in thymic macrophages by targeting Rictor is associated with suppression of the unique molecular signature of EIMP elucidated *in vitro*. These combined data indicate that EIMP occurs in high-AC setting *in vivo*.

EIMP contributes to AC Clearance and tissue protection *in vivo*

We first examined the resolution-related consequences of myeloid-Rictor deletion in the above dex-thymus model. As predicted by our hypothesis on the role of EIMP in continual efferocytosis, the thymi of Rictor-deficient dex-mice had an increase number of ACs compared with control dex-mice, and this was accompanied by increased overall cellularity and thymus weight (Figure 6D), which are features of thymi in which clearance of dead thymocytes is impaired (Park et al., 2011; Yurdagul et al., 2020). More directly, efferocytosis itself was impaired in the thymi of Rictor-deficient dex-mice (Figure 6E), which suggests a defect in continual efferocytosis in view of finding in Figure S3K that Rictor silencing in macrophages does not lower initial AC uptake. Most importantly, the impairments in EIMP and efferocytosis in Rictor-deficient dex-mice were associated with increased thymic necrosis and increased expression of the inflammatory cytokine IL-6, indicating impaired tissue resolution (Figures 6F, 6G, and S5E).

We next turned to a pre-clinical model of an important pro-resolving process in humans, atherosclerosis regression. In humans with established high-risk atherosclerosis, marked lowering of plasma cholesterol promotes features of plaque stabilization, notably decreases in plaque necrosis and thickening of a protective fibrous cap that overlies necrotic lesions, which is associated with lower risk of coronary artery disease (Sipahi et al., 2006). Hypercholesterolemic mice whose plasma cholesterol is markedly lowered provide a model of this plaque resolution process (Fisher, 2016). Moreover, efferocytosis by lesional

Gr1, indicating that the Gr1 is intracellular, i.e., a marker of macrophage engulfment of neutrophils. Right, flow plots and quantification of the percentage of EdU^+ cells within $F4/80^+$ macrophages that were either negative (AC^-) or positive (AC^+) for intracellular Gr1 (n = 5 mice per group).

(F) Ki67, Mac2, and TUNEL staining of thymic sections from mice 18 h after injection with PBS or dexamethasone (dex). The percentage of $Ki67^+$ macrophages among AC^+ and AC^- thymic macrophages was quantified by immunofluorescence microscopy (IFM) (n = 7 mice per group). Scale bar, 50 μm. All values are means ± SEM; letters that are different indicate statistical significance at $p < 0.05$.

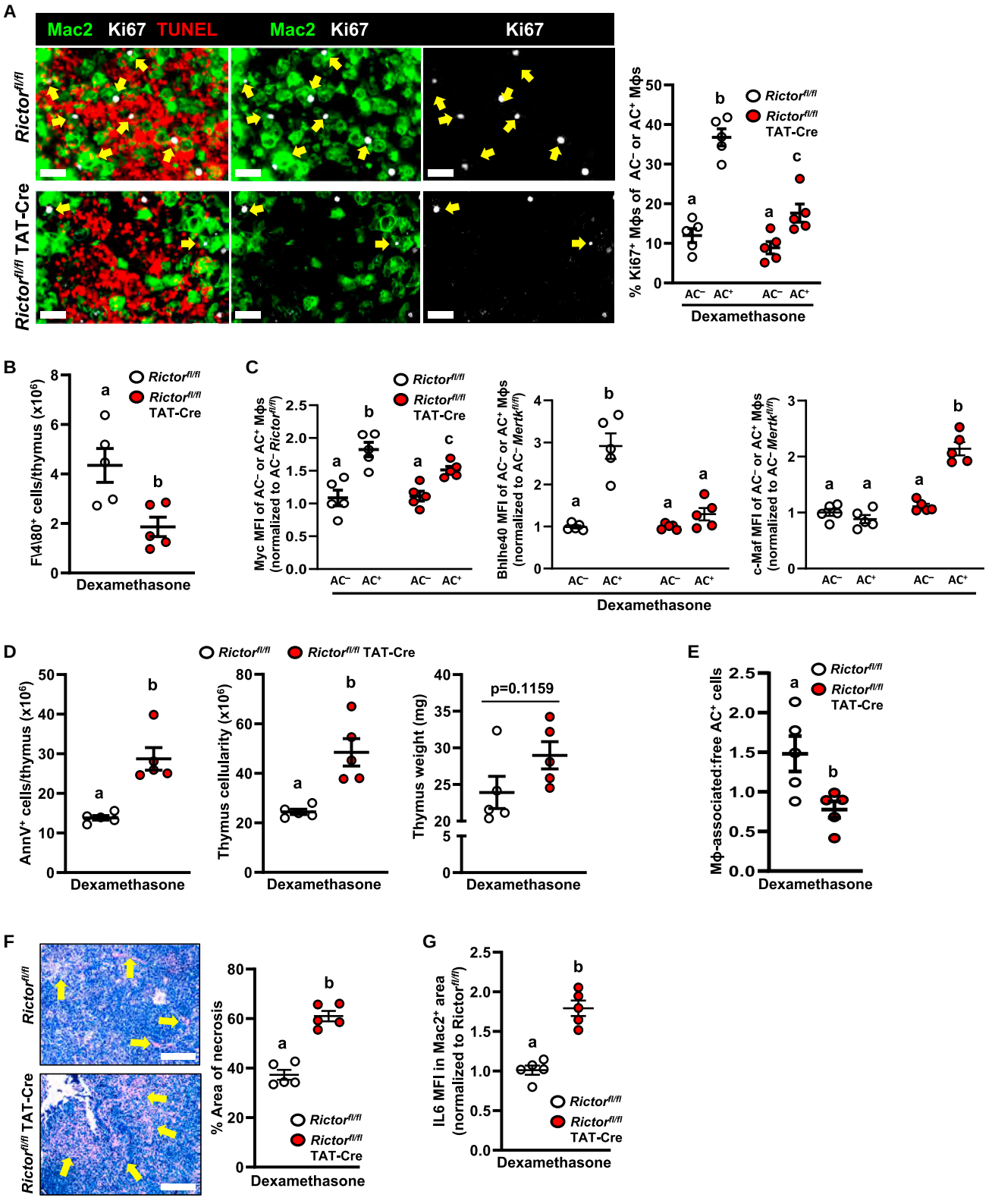

(legend on next page)

macrophages is increased during plaque regression and is a key process in the plaque remodeling/resolution response (Sharma et al., 2020; Yurdagul et al., 2020). For the regression model, *Ldlr*$^{-/-}$ mice are fed a Western-type diet for 16 weeks, which causes advanced atherosclerotic lesions at the aortic root. One cohort is harvested at this time (baseline) while others are injected with a helper-dependent adenovirus containing the human *LDLR* gene (HDAd-LDLR), which is non-integrating and restores LDL receptor expression in hepatocytes to clear plasma LDL, and then switched to a chow diet for 5 additional weeks (Willecke et al., 2015; Yurdagul et al., 2020).

To test the role of the AC-nucleotide-mTORC2 signaling pathway in atherosclerotic lesional macrophages at the time of regression, we took advantage of an approach that uses siRNA-containing nanoparticles (NPs) to silence genes in these cells (Tao et al., 2020). The NPs are conjugated with a peptide called S2P, which recognizes the macrophage receptor stabilin-2 and facilitates macrophage targeting, and they penetrate atherosclerotic lesions (Tao et al., 2020). The size and zeta potential of these NPs (Figures S6A and S6B) were similar to those in our previous report (Tao et al., 2020). The mice were injected at the onset of regression with S2P-NPs containing control scrambled RNA or siRNA targeting either of two mRNAs critical for the AC-nucleotide/mTORC2 signaling pathway, *Rictor* and *DNase2a*.

Beginning with siRictor NPs, the regression protocol successfully lowered plasma cholesterol in both cohorts (scrambled RNA and siRictor) compared with the baseline 16-week cohort (Figure S6C). Other systemic parameters in the regression cohorts were not affected significantly by siRictor NP administration (Figures S6D–S6H). As designed, siRictor NPs markedly lowered Rictor expression in regressing lesional macrophages (Mac2^{+}) but not in non-macrophage (Mac2^{-}) cells (Figure S6I). We found that efferocytosing (AC^{+}) macrophages in regressing lesions had a marked increase in Ki67-staining compared with either AC^{-} macrophages in these lesions or all macrophages in the baseline cohort (Figures 7A [first 4 groups] and S6J [first two columns of images]). Most importantly, this increase in Ki67 among AC^{+} macrophages in regressing lesions was markedly abrogated in the siRictor cohort (Figures 7A [groups 5 and 6] and S6J [third column of images]). As expected, the overall number of lesional macrophages was decreased by regression, but there was a selective increase in the subpopulation of macrophages carrying out efferocytosis (AC^{+}), which was abrogated by treatment with siRictor NPs (Figure 7B). We also found that Myc expression was increased in regressing lesional macrophages compared with baseline lesional macrophages, and the fold-increase was greater in AC^{+} versus AC^{-} macrophages; this finding was also abrogated by siRictor treatment (Figure 7C).

As noted above, efferocytosis increases in plaque regression (Sharma et al., 2020; Yurdagul et al., 2020), and we predicted that EIMP would enhance continual efferocytosis and the clearance of ACs in this setting by expanding the pool of efferocytes. Compared with baseline lesions, the ratio of macrophage-associated ACs:free ACs was increased in the control regression cohort, but not in the siRictor cohort, and this was associated with lowering of ACs in the control cohort, but not in the siRictor cohort, without a change in total ACs (Figures 7D and S6L). Most importantly, the decreases in plaque necrosis and lesion area and the increase in fibrous cap thickness observed in the control regressing lesions were abrogated by siRictor-NP treatment (Figures 7E and S6M).

In addition to blocking EIMP, two other effects of siRictor might have contributed to these plaque changes. First, in IL-4-treated macrophages *in vitro* and in worm-infected mice, deletion of Rictor lowers interferon regulatory factor 4 (IRF4), which, by suppressing oxidative phosphorylation, blocks macrophage alternative activation (Huang et al., 2016). Second, in the context that siRictor lowers Myc, Myc induces a set of specific genes in IL4-treated macrophages *in vitro*, notably *Alox15* and *Scarb1* (encoding SR-BI) that are associated with alternative activation (Pello et al., 2012). However, a recent study showed that IL-4 is not increased in regressing versus progressing lesions (Weinstock et al., 2021), and, most importantly, we found that treatment with siRictor NPs did not decrease arginase 1 (Arg1), which is a marker of alternatively activated macrophages, IRF4, ALOX15, or SR-BI in regressing lesional macrophages (Figure S6N).

To provide further evidence for the nucleotide-EIMP pathway in plaque regression, we tested the effect of S2P-NPs containing siDNase2a. siDNase2a NPs did not have a significant effect on cholesterol or other systemic endpoints during regression (Figures S7A–S7F), and they successfully lowered DNase2a expression in regressing lesional macrophages, but not in non-macrophage cells (Figure S7G). Compared with scrambled RNA-NP treatment, siDNase2a-NP treatment lowered Ki67-positivity in efferocytosing (AC^{+}) macrophages in regressing lesions, abrogated the expansion of efferocytosing macrophages in regression, and lowered Myc expression to a greater degree in AC^{+} versus AC^{-} macrophages (Figures 7F–7H and S7H). These changes were associated with impairments in regression-induced efferocytosis and AC clearance, regression-induced

Figure 6. Rictor-dependent EIMP and resolution in dexamethasone-induced thymocyte apoptosis

Mice were transplanted with *Rictor*$^{fl/fl}$ and *Rictor*$^{fl/fl}$ TAT-Cre bone marrow. After 4 weeks, the mice were injected i.p. with PBS or dexamethasone (dex), and then the thymi were harvested 18 h later and assayed as follows:

(A) Ki67, Mac2, and TUNEL staining, with yellow arrows indicating Mac2^{+} Ki67^{+} AC^{+} macrophages. Scale bar, 50 μm. The graph shows quantification of percentage of Ki67^{+} cells within AC^{+} and AC^{-} macrophages (n = 5 mice per group). Scale bar, 50 μm.

(B) Quantification of F4/80^{+} macrophages by flow cytometry (n = 5 mice per group).

(C) Quantification by IFM of Myc, Bhlhe40, and c-Maf MFI in AC^{+} and AC^{-} macrophages (n = 5 mice per group).

(D) Annexin-V^{+} (apoptotic) cells by flow cytometry and cell counting, and thymic weights (n = 5 mice per group).

(E) As a measure of efferocytosis, ratio of Mac2^{+} macrophage-associated:free TUNEL^{+} ACs by IFM (n = 5 mice per group).

(F) Quantification of percent area of necrosis (anuclear area) of total area in H&E-stained sections; yellow arrows indicate area of necrosis (n = 5 mice per group). Scale bar, 200 μm.

(G) Immunostaining and quantification of IL-6 MFI in Mac2^{+} areas (n = 5 mice per group).

All values are means ± SEM; letters that are different indicate statistical significance at $p < 0.05$.

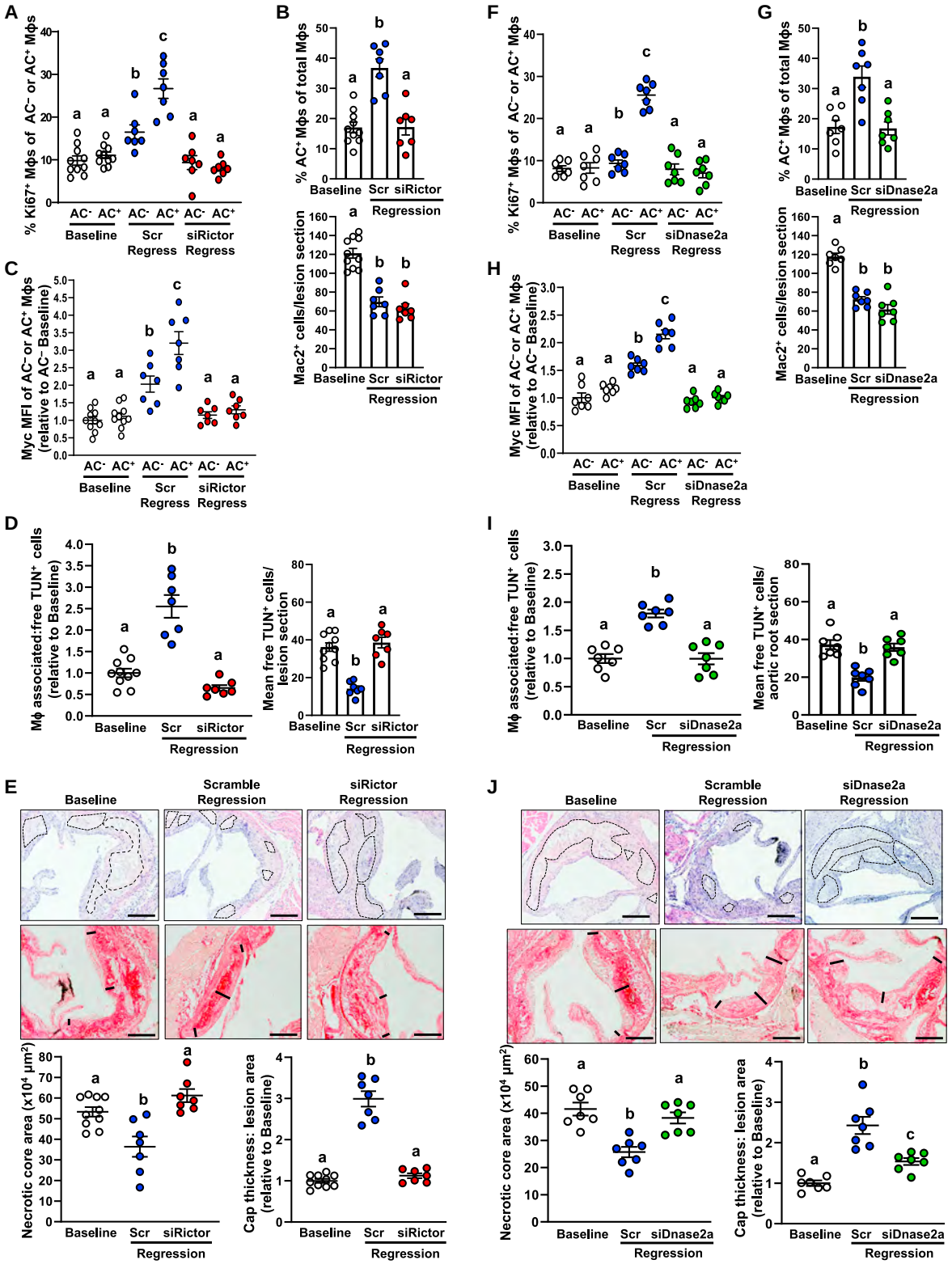

Figure 7. Rictor- and DNase2a-dependent EIMP and resolution in atherosclerosis regression

Ldlr$^{-/-}$ mice were fed the Western diet for 16 weeks and then either harvested (baseline) or subjected to the atherosclerosis-regression protocol for 5 weeks. The regression mice were administered S2P-NPs containing siRictor (A–E) or siDNase2a (F–J) (or scrambled-RNA NPs as control), throughout the regression period.

(legend continued on next page)

decreases in plaque necrosis and lesion area, and regression-induced fibrous cap thickening (Figures 7I, 7J, and S7H–S7J). As with siRictor, the expression of Arg1, IRF4, ALOX15, and SR-BI in regressing lesional macrophages was not affected by siDNase2a (Figure S7K). Finally, the impairments in the resolution in the siDNase2a cohort could, in theory, be caused by activation of a stimulator-of-interferon-genes (STING) response in macrophages. However, we found that the expression of the chemokine CXCL10, a marker of the STING response *in vivo* (Okabe et al., 2005), was very low in regressing lesional macrophages and not affected by siDNase2a-NP treatment (Figure S7L). Further, *Cxcl10* mRNA actually decreased in AC-incubated BMDMs 4 h after AC removal and was not affected by siDNase2a despite the fact that EIMP occurs in this time frame and is suppressed by siDNase2a (Figure S7M). While siDNase2a did increase *Cxcl10* 24 h after an initial AC exposure, silencing STING did not rescue the inhibitory effect of siDNase2a on EIMP despite successfully lowering *Cxcl10* (Figures S7N and S7O). These combined data show that the inhibition of EIMP by siDNase2a is not a secondary effect of a STING-mediated type 1 interferon response. In summary, proliferation is observed in efferocytosing macrophages in regressing atherosclerotic lesions, and silencing two different molecules in the nucleotide-mTORC2-EIMP pathway in macrophages blocks this proliferative response and abrogates key regression-induced resolution processes important to plaque stabilization.

DISCUSSION

Based on the findings here and in previous reports (A-Gonzalez et al., 2009; Morioka et al., 2018; Yurdagul et al., 2020; Zhang et al., 2019), we propose an integrated resolution concept related to AC-cargo pathways in efferocytosing macrophages: while most pathways (e.g., those stimulated by AC-derived amino acids and lipids) promote resolution in individual macrophages, EIMP triggered by AC-derived nucleotides *amplifies* this effect by expanding the pool of these resolving macrophages. As continuing efferocytosis is a key pro-resolving function in these pathways, a positive-feedback cycle is established to handle high-AC burdens and prevent tissue injury. As a consequence, when any step in this cycle is interrupted in a disease setting, a pathogenic negative-feedback cycle of impaired resolution and efferocytosis ensues (Dalli and Serhan, 2017; Doran et al., 2020; Morioka et al., 2019).

Two key lines of evidence suggest that EIMP is a key contributing factor to the beneficial resolution-efferocytosis cycle. First, the expanded pool of macrophages resulting from EIMP are highly competent at both continual efferocytosis and post-efferocytic production of TGFβ and IL-10. Second, interruption of the EIMP signaling pathway *in vivo* causes a decrease in efferocytic (AC^+) macrophage proliferation and, most importantly, this is associated with impaired resolution and AC clearance. A key point when we conducted this experiment in atherosclerosis regression was that almost identical results were obtained when we silenced either of two distinct molecules in the pathway, Rictor or DNase2a, which have not previously been linked together in other cellular pathways. Of note, a previous study reported that overall macrophage proliferation is reduced during plaque regression (Härdtner et al., 2020), and we, as others (Sharma et al., 2020), found a net overall decrease in the total number of macrophages in regressing versus baseline plaques. The key point revealed here, however, is that proliferation is increased in a subpopulation of macrophages in these lesions, i.e., efferocytosing macrophages, suggesting that the combination of these processes is to increase the resolving:inflammatory macrophage ratio in regression to promote plaque stabilization.

Future studies will determine if interruption of additional processes contributes to impaired resolution when the AC-nucleotide-mTORC2 pathway is silenced in macrophages *in vivo*. One theoretical possibility is that activation of Rictor and/or Myc in the pathway could promote the alternative activation of macrophages, which is seen in high IL-4 settings *in vitro* and *in vivo* (Huang et al., 2016; Pello et al., 2012). However, resolving plaques do not have higher levels of IL-4 or the related cytokine IL-13 than progressing plaques (Weinstock et al., 2021), and we did not detect evidence of these pathways in regressing lesional macrophages. Thus, context is key, which is further highlighted by the *anti*-atherogenic effect of myeloid Rictor deletion in the very different setting of progressing atherosclerosis (Babaev et al., 2018). In particular, progressing lesions are populated with inflammatory macrophages (Rahman et al., 2017), which we showed do not respond to efferocytosis with proliferation.

Elegant prior reports have demonstrated macrophage proliferation in other settings, but in these settings, proliferation was not linked to AC engulfment or shown to be a mechanism to increase AC-clearance capacity. For example, tissue-resident macrophages established during embryogenesis are able to self-renew to restore tissue homeostasis (Alliot et al., 1999; Davies et al., 2011; Hashimoto et al., 2013). One mediator of macrophage self-renewal is CSF1 (Fejer et al., 2015), which we showed triggers proliferation by a pathway that is distinct from the EIMP

(A and F) Lesions were immunostained for Ki67, Mac2, and TUNEL. Overlap of cytoplasmic TUNEL staining with $Mac2^+$ macrophages indicates efferocytosing (AC^+) macrophages. The percent $Ki67^+$ macrophages within AC^+ and AC^- lesional macrophages was quantified by IFM (n = 7–10 mice per group).
(B and G) The percent of efferocytosing (AC^+) macrophages among total macrophages and the total number of $Mac2^+$ cells per lesion section were quantified in the three groups of mice.
(C and H) Lesions were immunostained for Myc, Mac2, and TUNEL. Myc MFI within AC^+ and AC^- lesional macrophages was quantified by IFM and expressed relative to the MFI of Myc in AC^- macrophages in the baseline cohort (n = 7–10 mice per group).
(D and I) Left, quantification of the ratio of macrophage-associated ACs:free ACs, expressed relative to the baseline cohort. Right, the mean number of apoptotic (nuclear $TUNEL^+$) cells per aortic root lesion section.
(E and J) Quantification of the lesions for necrotic area and fibrous cap thickness. The images on the top row are H&E-stained; necrotic areas are outlined with dashed lines. The images on the bottom row of images Sirius red-stained and show where fibrous cap thickness was measured. Scale bar, 200 μm. Collagen cap thickness was measured at the lesional midpoint and both shoulder regions and then averaged and quantified as the ratio of collagen cap thickness to lesion area; data are presented relative to the baseline cohort average.
All values are means ± SEM; letters that are different indicate statistical significance at $p < 0.05$.

pathway. A previous *in vitro* study reported that ACs can support the survival of growth factor-starved macrophages while actually inhibiting CSF1-induced macrophage proliferation (Reddy et al., 2002), but whether these phenomena are relevant *in vivo*, particularly in settings of high-burden apoptosis, remains unknown. Other important studies have shown that macrophage proliferation occurs in settings of Th2 immunity, such as in response to IL-4 *in vitro* or helminth infection *in vivo* (Bosurgi et al., 2017; Jarjour et al., 2019; Jenkins et al., 2011). In one of these studies, combined deletion of MerTK and Axl was shown to suppress macrophage proliferation in worm-infected mice (Bosurgi et al., 2017), but the proliferative response was not linked to AC engulfment or metabolism, ERK1/2-Myc signaling, or AC clearance *in vivo*. While it is possible that the findings in this previous study may have relevance to the MerTK arm of EIMP, Th2-induced macrophage proliferation requires IL-4 (Bosurgi et al., 2017), whereas EIMP does not. Finally, in a completely different scenario, inflammation can be a stimulus for pathogenic macrophage proliferation, including in progressing atherosclerosis (Davies et al., 2013; Du et al., 2020; Morita et al., 2020; Robbins et al., 2013; Sinha et al., 2021). We found that IFNγ−/LPS-treated macrophages were unable to execute EIMP, which may be related to the finding that LPS suppresses Myc expression in macrophages (Liu et al., 2016). Moreover, the proliferation of inflammatory macrophages in progressing lesions is induced by CSF1 (Sinha et al., 2021), which, as mentioned, is distinct from EIMP.

In chronic, non-resolving diseases, efferocytosis is impaired, which, based on our findings, would block the efferocytosis-resolution-EIMP positive-feedback cycle and amplify disease progression. Progressing atherosclerosis is a prime example in which this cycle is likely to be broken by processes known to block lesional macrophage efferocytosis, such as MerTK cleavage or SIRPα activation (Cai et al., 2017; Kojima et al., 2016). Moreover, these lesions are populated mostly by inflammatory macrophages, which are incapable of EIMP. However, these lesions do contain a small population of non-inflammatory, efferocytic macrophages, and so, based on the mechanisms identified herein, it may be possible to therapeutically promote the specific expansion of this population of macrophages to restore the pro-resolving positive-feedback cycle.

Limitations of the study

In addition to blocking EIMP, siDNase2a and siRictor could have affected our *in vivo* endpoints by one or more additional mechanisms. In our analysis of the atherosclerosis regression model, we presented data suggesting that certain key possible confounders (e.g., changes in macrophage polarization or IRF4 for siRictor or a type-1 IFN response for siDNase2a) were not triggered by the siRNAs. Moreover, the fact that almost identical results were observed for both siRNAs further suggests the effects seen were due primarily to interruption of EIMP. Nonetheless, a future study looking at the effects of these interventions on lesional cell populations and gene expression, e.g., via single-cell sequencing, could add further insight into this issue. Further, it would, in theory, be helpful to test an intervention that directly blocked macrophage cell cycling, i.e., without blocking an upstream signaling pathway, as long as that intervention did not have its own confounding issues (e.g., blocking monocyte generation in the bone marrow, blocking inflammatory macrophage proliferation, or triggering cell senescence). The most impactful test of our central hypothesis on the pro-resolving role of EIMP was in a mouse model of atherosclerosis regression. While this model phenocopies certain plaque stabilization features in humans after marked lowering of plasma LDL, the results of our study do not address whether the pathway plays a role in atherosclerosis regression in humans or contributes to the lowering of CAD risk in this setting. Future studies comparing stable with unstable regions of human atheroma for the biochemical signature of the pathway, viewed in the context of our data showing that the pathway is present in HMDMs, may add increased human relevance to these findings.

STAR★METHODS

Detailed methods are provided in the online version of this paper and include the following:

- KEY RESOURCES TABLE
- RESOURCE AVAILABILITY
  - Lead contact
  - Materials availability
  - Data and code availability
- EXPERIMENTAL MODEL AND SUBJECT DETAILS
  - Cell lines
  - Primary cell culture
  - Human samples
  - Mouse studies
- METHOD DETAILS
  - Induction of apoptosis and fluorescent labeling of Jurkat cells
  - siRNA-mediated gene silencing
  - Efferocytosis-induced macrophage proliferation assay and flow cytometry
  - Cell number counting
  - CFSE proliferation assay
  - Assay of single-AC and sequential double-AC uptake by control macrophages and EIMP-induced proliferative macrophages
  - Nuclear EdU incorporation assay
  - Assay of TGFβ and IL-10 by EIMP-induced proliferative macrophages
  - Zymosan-induced peritonitis and peritoneal uptake of labeled ACs
  - Bone marrow transplant
  - Thymus assays
  - siRictor and siDnase2a S2P-nanoparticles
  - Tissue collection and lesion analysis
  - Tissue immunohistochemistry and immunofluorescence microscopy
  - Immunoblotting
  - Quantitative real time PCR
  - Electroporation of overexpression plasmids
- QUANTIFICATION AND STATISTICAL ANALYSIS

SUPPLEMENTAL INFORMATION

Supplemental information can be found online at https://doi.org/10.1016/j.cmet.2021.10.015.

ACKNOWLEDGMENTS

We thank Dr. Carla Rothlin for providing *Mertk*$^{fl/fl}$ mice and Drs. Theresa Swayne and Laura Munteanu for assistance with confocal imaging. The confocal microscopy work in this study was conducted in the Confocal and Specialized Microscopy Shared Resource of the Herbert Irving Comprehensive Cancer Center at Columbia University, supported by NIH grants P30CA013696 and S10RR025686. Flow cytometry was conducted in the Columbia Center for Translational Immunology Core Facility, funded by NIH grants P30CA013696, S10OD020056, and S10RR027050. Co-authors were supported by the following NIH grants: T32 5T32HL007343-42 to B.D.G.; K99 HL145131 to A.Y.,Jr.; P20 GM121307 to C.G.K.; R01 HL127464 to I.T. and J.S.; and R01 HL087123 and R35 HL145228 to I.T. This work was also supported by an American Heart Association post-doctoral fellowship grant (20POST35210962 to C.K.), Harvard Medical School (HMS)/Brigham and Women's Hospital (BWH) Khoury Innovation award (122829 to W.T.), and an Assistant Professor start-up package from HMS/BWH Department of Anesthesiology, Perioperative and Pain Medicine to W.T.

AUTHOR CONTRIBUTIONS

B.D.G., P.B.A., A.Y.,Jr., M.C.L., and I.T. developed the study concept and experimental design; B.D.G., P.B.A., A.Y.,Jr., and M.C.L. conducted the experiments; A.Y.,Jr., P.B.A., X.W., and C.K. assisted with the bone marrow transplants and the dexamethasone-thymus and zymosan-peritonitis models; W.T. designed siRNA nanoparticles; and J.S. was involved in the original concept of these nanoparticles. C.L. and N.K. synthesized and characterized all the siRNA nanoparticles under the guidance of W.T. B.D.G., P.B.A., and I.T. wrote the manuscript, and the other co-authors provided comments and revisions.

DECLARATION OF INTERESTS

The authors declare no competing interests.

Received: March 23, 2021
Revised: August 17, 2021
Accepted: October 26, 2021
Published: November 15, 2021

REFERENCES

A-Gonzalez, N., Bensinger, S.J., Hong, C., Beceiro, S., Bradley, M.N., Zelcer, N., Deniz, J., Ramirez, C., Díaz, M., Gallardo, G., et al. (2009). Apoptotic cells promote their own clearance and immune tolerance through activation of the nuclear receptor LXR. Immunity *31*, 245–258.

Alliot, F., Godin, I., and Pessac, B. (1999). Microglia derive from progenitors, originating from the yolk sac, and which proliferate in the brain. Brain Res. Dev. Brain Res. *117*, 145–152.

Babaev, V.R., Huang, J., Ding, L., Zhang, Y., May, J.M., and Linton, M.F. (2018). Loss of Rictor in monocyte/macrophages suppresses their proliferation and viability reducing atherosclerosis in LDLR null mice. Front. Immunol. *9*, 215.

Bagaitkar, J., Huang, J., Zeng, M.Y., Pech, N.K., Monlish, D.A., Perez-Zapata, L.J., Miralda, I., Schuettpelz, L.G., and Dinauer, M.C. (2018). NADPH oxidase activation regulates apoptotic neutrophil clearance by murine macrophages. Blood *131*, 2367–2378.

Boada-Romero, E., Martinez, J., Heckmann, B.L., and Green, D.R. (2020). The clearance of dead cells by efferocytosis. Nat. Rev. Mol. Cell Biol. *21*, 398–414.

Bosurgi, L., Cao, Y.G., Cabeza-Cabrerizo, M., Tucci, A., Hughes, L.D., Kong, Y., Weinstein, J.S., Licona-Limon, P., Schmid, E.T., Pelorosso, F., et al. (2017). Macrophage function in tissue repair and remodeling requires IL-4 or IL-13 with apoptotic cells. Science *356*, 1072–1076.

Cai, B., Thorp, E.B., Doran, A.C., Subramanian, M., Sansbury, B.E., Lin, C.S., Spite, M., Fredman, G., and Tabas, I. (2016). MerTK cleavage limits proresolving mediator biosynthesis and exacerbates tissue inflammation. Proc. Natl. Acad. Sci. USA *113*, 6526–6531.

Cai, B., Thorp, E.B., Doran, A.C., Sansbury, B.E., Daemen, M.J., Dorweiler, B., Spite, M., Fredman, G., and Tabas, I. (2017). MerTK receptor cleavage promotes plaque necrosis and defective resolution in atherosclerosis. J. Clin. Invest. *127*, 564–568.

Cai, B., Kasikara, C., Doran, A.C., Ramakrishnan, R., Birge, R.B., and Tabas, I. (2018). MerTK signaling in macrophages promotes the synthesis of inflammation resolution mediators by suppressing CaMKII activity. Sci. Signal. *11*, eaar3721.

Cai, B., Dongiovanni, P., Corey, K.E., Wang, X., Shmarakov, I.O., Zheng, Z., Kasikara, C., Davra, V., Meroni, M., Chung, R.T., et al. (2020). Macrophage MerTK promotes liver fibrosis in nonalcoholic steatohepatitis. Cell Metab. *31*, 406–421.e7.

Camenisch, T.D., Koller, B.H., Earp, H.S., and Matsushima, G.K. (1999). A novel receptor tyrosine kinase, Mer, inhibits TNF-alpha production and lipopolysaccharide-induced endotoxic shock. J. Immunol. *162*, 3498–3503.

Carroll, P.A., Freie, B.W., Mathsyaraja, H., and Eisenman, R.N. (2018). The MYC transcription factor network: balancing metabolism, proliferation and oncogenesis. Front. Med. *12*, 412–425.

Dalli, J., and Serhan, C.N. (2017). Pro-resolving mediators in regulating and conferring macrophage function. Front. Immunol. *8*, 1400.

Davies, L.C., Rosas, M., Smith, P.J., Fraser, D.J., Jones, S.A., and Taylor, P.R. (2011). A quantifiable proliferative burst of tissue macrophages restores homeostatic macrophage populations after acute inflammation. Eur. J. Immunol. *41*, 2155–2164.

Davies, L.C., Rosas, M., Jenkins, S.J., Liao, C.T., Scurr, M.J., Brombacher, F., Fraser, D.J., Allen, J.E., Jones, S.A., and Taylor, P.R. (2013). Distinct bone marrow-derived and tissue-resident macrophage lineages proliferate at key stages during inflammation. Nat. Commun. *4*, 1886.

Doran, A.C., Yurdagul, A., Jr., and Tabas, I. (2020). Efferocytosis in health and disease. Nat. Rev. Immunol. *20*, 254–267.

Du, L.J., Sun, J.Y., Zhang, W.C., Wang, Y.L., Zhu, H., Liu, T., Gao, M.Z., Zheng, C., Zhang, Y.Y., Liu, Y., et al. (2020). Macrophage NCOR1 deficiency ameliorates myocardial infarction and neointimal hyperplasia in mice. J. Am. Heart Assoc. *9*, e015862.

Dynan, W.S., and Yoo, S. (1998). Interaction of Ku protein and DNA-dependent protein kinase catalytic subunit with nucleic acids. Nucleic Acids Res. *26*, 1551–1559.

Fadok, V.A., Bratton, D.L., Konowal, A., Freed, P.W., Westcott, J.Y., and Henson, P.M. (1998). Macrophages that have ingested apoptotic cells in vitro inhibit proinflammatory cytokine production through autocrine/paracrine mechanisms involving TGF-β, PGE2, and PAF. J. Clin. Invest. *101*, 890–898.

Favata, M.F., Horiuchi, K.Y., Manos, E.J., Daulerio, A.J., Stradley, D.A., Feeser, W.S., Van Dyk, D.E., Pitts, W.J., Earl, R.A., Hobbs, F., et al. (1998). Identification of a novel inhibitor of mitogen-activated protein kinase kinase. J. Biol. Chem. *273*, 18623–18632.

Fejer, G., Sharma, S., and Gyory, I. (2015). Self-renewing macrophages–a new line of enquiries in mononuclear phagocytes. Immunobiology *220*, 169–174.

Fisher, E.A. (2016). Regression of atherosclerosis: The journey from the liver to the plaque and back. Arterioscler. Thromb. Vasc. Biol. *36*, 226–235.

Fourgeaud, L., Través, P.G., Tufail, Y., Leal-Bailey, H., Lew, E.D., Burrola, P.G., Callaway, P., Zagórska, A., Rothlin, C.V., Nimmerjahn, A., and Lemke, G. (2016). TAM receptors regulate multiple features of microglial physiology. Nature *532*, 240–244.

Härdtner, C., Kornemann, J., Krebs, K., Ehlert, C.A., Jander, A., Zou, J., Starz, C., Rauterberg, S., Sharipova, D., Dufner, B., et al. (2020). Inhibition of macrophage proliferation dominates plaque regression in response to cholesterol lowering. Basic Res. Cardiol. *115*, 78.

Hashimoto, D., Chow, A., Noizat, C., Teo, P., Beasley, M.B., Leboeuf, M., Becker, C.D., See, P., Price, J., Lucas, D., et al. (2013). Tissue-resident macrophages self-maintain locally throughout adult life with minimal contribution from circulating monocytes. Immunity *38*, 792–804.

Henson, P.M. (2017). Cell Removal: Efferocytosis. Annu. Rev. Cell Dev. Biol. *33*, 127–144.

Huang, S.C., Smith, A.M., Everts, B., Colonna, M., Pearce, E.L., Schilling, J.D., and Pearce, E.J. (2016). Metabolic reprogramming mediated by the mTORC2-IRF4 signaling axis is essential for macrophage alternative activation. Immunity *45*, 817–830.

Jarjour, N.N., Schwarzkopf, E.A., Bradstreet, T.R., Shchukina, I., Lin, C.C., Huang, S.C., Lai, C.W., Cook, M.E., Taneja, R., Stappenbeck, T.S., et al. (2019). Bhlhe40 mediates tissue-specific control of macrophage proliferation in homeostasis and type 2 immunity. Nat. Immunol. *20*, 687–700.

Jenkins, S.J., Ruckerl, D., Cook, P.C., Jones, L.H., Finkelman, F.D., van Rooijen, N., MacDonald, A.S., and Allen, J.E. (2011). Local macrophage proliferation, rather than recruitment from the blood, is a signature of TH2 inflammation. Science *332*, 1284–1288.

Kamaly, N., Fredman, G., Subramanian, M., Gadde, S., Pesic, A., Cheung, L., Fayad, Z.A., Langer, R., Tabas, I., and Farokhzad, O.C. (2013). Development and in vivo efficacy of targeted polymeric inflammation-resolving nanoparticles. Proc. Natl. Acad. Sci. USA *110*, 6506–6511.

Kojima, Y., Volkmer, J.P., McKenna, K., Civelek, M., Lusis, A.J., Miller, C.L., Direnzo, D., Nanda, V., Ye, J., Connolly, A.J., et al. (2016). CD47-blocking antibodies restore phagocytosis and prevent atherosclerosis. Nature *536*, 86–90.

Lan, Y.Y., Londoño, D., Bouley, R., Rooney, M.S., and Hacohen, N. (2014). Dnase2a deficiency uncovers lysosomal clearance of damaged nuclear DNA via autophagy. Cell Rep. *9*, 180–192.

Lemke, G., and Rothlin, C.V. (2008). Immunobiology of the TAM receptors. Nat. Rev. Immunol. *8*, 327–336.

Liu, L., Lu, Y., Martinez, J., Bi, Y., Lian, G., Wang, T., Milasta, S., Wang, J., Yang, M., Liu, G., et al. (2016). Proinflammatory signal suppresses proliferation and shifts macrophage metabolism from Myc-dependent to HIF1α-dependent. Proc. Natl. Acad. Sci. USA *113*, 1564–1569.

Martinez, J., Malireddi, R.K., Lu, Q., Cunha, L.D., Pelletier, S., Gingras, S., Orchard, R., Guan, J.L., Tan, H., Peng, J., et al. (2015). Molecular characterization of LC3-associated phagocytosis reveals distinct roles for Rubicon, NOX2 and autophagy proteins. Nat. Cell Biol. *17*, 893–906.

McDonald, P.P., Fadok, V.A., Bratton, D., and Henson, P.M. (1999). Transcriptional and translational regulation of inflammatory mediator production by endogenous TGF-beta in macrophages that have ingested apoptotic cells. J. Immunol. *163*, 6164–6172.

Minchew, C.L., and Didenko, V.V. (2011). Fluorescent probes detecting the phagocytic phase of apoptosis: enzyme-substrate complexes of topoisomerase and DNA. Molecules *16*, 4599–4614.

Morioka, S., Perry, J.S.A., Raymond, M.H., Medina, C.B., Zhu, Y., Zhao, L., Serbulea, V., Onengut-Gumuscu, S., Leitinger, N., Kucenas, S., et al. (2018). Efferocytosis induces a novel SLC program to promote glucose uptake and lactate release. Nature *563*, 714–718.

Morioka, S., Maueröder, C., and Ravichandran, K.S. (2019). Living on the edge: Efferocytosis at the interface of homeostasis and pathology. Immunity *50*, 1149–1162.

Morita, Y., Senokuchi, T., Yamada, S., Wada, T., Furusho, T., Matsumura, T., Ishii, N., Nishida, S., Nishida, S., Motoshima, H., et al. (2020). Impact of tissue macrophage proliferation on peripheral and systemic insulin resistance in obese mice with diabetes. BMJ Open Diabetes Res. Care *8*, e001578.

Nishi, C., Yanagihashi, Y., Segawa, K., and Nagata, S. (2019). MERTK tyrosine kinase receptor together with TIM4 phosphatidylserine receptor mediates distinct signal transduction pathways for efferocytosis and cell proliferation. J. Biol. Chem. *294*, 7221–7230.

O'Neill, L.A., and Pearce, E.J. (2016). Immunometabolism governs dendritic cell and macrophage function. J. Exp. Med. *213*, 15–23.

Okabe, Y., Kawane, K., Akira, S., Taniguchi, T., and Nagata, S. (2005). Toll-like receptor-independent gene induction program activated by mammalian DNA escaped from apoptotic DNA degradation. J. Exp. Med. *202*, 1333–1339.

Park, D., Han, C.Z., Elliott, M.R., Kinchen, J.M., Trampont, P.C., Das, S., Collins, S., Lysiak, J.J., Hoehn, K.L., and Ravichandran, K.S. (2011). Continued clearance of apoptotic cells critically depends on the phagocyte Ucp2 protein. Nature *477*, 220–224.

Pashover-Schallinger, E., Aswad, M., Schif-Zuck, S., Shapiro, H., Singer, P., and Ariel, A. (2012). The atypical chemokine receptor D6 controls macrophage efferocytosis and cytokine secretion during the resolution of inflammation. FASEB J. *26*, 3891–3900.

Pello, O.M., De Pizzol, M., Mirolo, M., Soucek, L., Zammataro, L., Amabile, A., Doni, A., Nebuloni, M., Swigart, L.B., Evan, G.I., et al. (2012). Role of c-MYC in alternative activation of human macrophages and tumor-associated macrophage biology. Blood *119*, 411–421.

Proto, J.D., Doran, A.C., Gusarova, G., Yurdagul, A., Jr., Sozen, E., Subramanian, M., Islam, M.N., Rymond, C.C., Du, J., Hook, J., et al. (2018). Regulatory T cells promote macrophage efferocytosis during inflammation resolution. Immunity *49*, 666–677.e6.

Rahman, K., Vengrenyuk, Y., Ramsey, S.A., Vila, N.R., Girgis, N.M., Liu, J., Gusarova, V., Gromada, J., Weinstock, A., Moore, K.J., et al. (2017). Inflammatory Ly6Chi monocytes and their conversion to M2 macrophages drive atherosclerosis regression. J. Clin. Invest. *127*, 2904–2915.

Rauschmeier, R., Gustafsson, C., Reinhardt, A., A-Gonzalez, N., Tortola, L., Cansever, D., Subramanian, S., Taneja, R., Rossner, M.J., Sieweke, M.H., et al. (2019). Bhlhe40 and Bhlhe41 transcription factors regulate alveolar macrophage self-renewal and identity. EMBO J. *38*, e101233.

Reddy, S.M., Hsiao, K.H., Abernethy, V.E., Fan, H., Longacre, A., Lieberthal, W., Rauch, J., Koh, J.S., and Levine, J.S. (2002). Phagocytosis of apoptotic cells by macrophages induces novel signaling events leading to cytokine-independent survival and inhibition of proliferation: activation of Akt and inhibition of extracellular signal-regulated kinases 1 and 2. J. Immunol. *169*, 702–713.

Robbins, C.S., Hilgendorf, I., Weber, G.F., Theurl, I., Iwamoto, Y., Figueiredo, J.L., Gorbatov, R., Sukhova, G.K., Gerhardt, L.M., Smyth, D., et al. (2013). Local proliferation dominates lesional macrophage accumulation in atherosclerosis. Nat. Med. *19*, 1166–1172.

Schlegel, J., Sambade, M.J., Sather, S., Moschos, S.J., Tan, A.C., Winges, A., DeRyckere, D., Carson, C.C., Trembath, D.G., Tentler, J.J., et al. (2013). MERTK receptor tyrosine kinase is a therapeutic target in melanoma. J. Clin. Invest. *123*, 2257–2267.

Sears, R., Leone, G., DeGregori, J., and Nevins, J.R. (1999). Ras enhances Myc protein stability. Mol. Cell *3*, 169–179.

Sharma, M., Schlegel, M.P., Afonso, M.S., Brown, E.J., Rahman, K., Weinstock, A., Sansbury, B.E., Corr, E.M., van Solingen, C., Koelwyn, G.J., et al. (2020). Regulatory T Cells license macrophage pro-resolving functions during atherosclerosis regression. Circ. Res. *127*, 335–353.

Sinha, S.K., Miikeda, A., Fouladian, Z., Mehrabian, M., Edillor, C., Shih, D., Zhou, Z., Paul, M.K., Charugundla, S., Davis, R.C., et al. (2021). Local M-CSF (macrophage colony-stimulating factor) expression regulates macrophage proliferation and apoptosis in atherosclerosis. Arterioscler. Thromb. Vasc. Biol. *41*, 220–233.

Sipahi, I., Nicholls, S.J., Tuzcu, E.M., and Nissen, S.E. (2006). Coronary atherosclerosis can regress with very intensive statin therapy. Cleve. Clin. J. Med. *73*, 937–944.

Subramanian, M., Proto, J.D., Matsushima, G.K., and Tabas, I. (2016). Deficiency of AXL in bone marrow-derived cells does not affect advanced atherosclerotic lesion progression. Sci. Rep. *6*, 39111.

Tao, W., Yurdagul, A., Jr., Kong, N., Li, W., Wang, X., Doran, A.C., Feng, C., Wang, J., Islam, M.A., Farokhzad, O.C., et al. (2020). siRNA nanoparticles targeting CaMKIIγ in lesional macrophages improve atherosclerotic plaque stability in mice. Sci. Transl. Med. *12*, eaay1063.

Tibrewal, N., Wu, Y., D'mello, V., Akakura, R., George, T.C., Varnum, B., and Birge, R.B. (2008). Autophosphorylation docking site Tyr-867 in Mer receptor tyrosine kinase allows for dissociation of multiple signaling pathways for phagocytosis of apoptotic cells and down-modulation of lipopolysaccharide-inducible NF-kappaB transcriptional activation. J. Biol. Chem. *283*, 3618–3627.

Voll, R.E., Herrmann, M., Roth, E.A., Stach, C., Kalden, J.R., and Girkontaite, I. (1997). Immunosuppressive effects of apoptotic cells. Nature *390*, 350–351.

Wang, Y., Subramanian, M., Yurdagul, A., Jr., Barbosa-Lorenzi, V.C., Cai, B., de Juan-Sanz, J., Ryan, T.A., Nomura, M., Maxfield, F.R., and Tabas, I. (2017).

Mitochondrial fission promotes the continued clearance of apoptotic cells by macrophages. Cell *171*, 331–345.e22.

Weinstock, A., Rahman, K., Yaacov, O., Nishi, H., Menon, P., Nikain, C.A., Garabedian, M.L., Pena, S., Akbar, N., Sansbury, B.E., et al. (2021). Wnt signaling enhances macrophage responses to IL-4 and promotes resolution of atherosclerosis. eLife *10*, e67932.

Willecke, F., Yuan, C., Oka, K., Chan, L., Hu, Y., Barnhart, S., Bornfeldt, K.E., Goldberg, I.J., and Fisher, E.A. (2015). Effects of high fat feeding and diabetes on regression of atherosclerosis induced by low-density lipoprotein receptor gene therapy in LDL receptor-deficient mice. PLoS ONE *10*, e0128996.

Wynn, T.A., Chawla, A., and Pollard, J.W. (2013). Macrophage biology in development, homeostasis and disease. Nature *496*, 445–455.

Xiong, W., Frasch, S.C., Thomas, S.M., Bratton, D.L., and Henson, P.M. (2013). Induction of TGF-β1 synthesis by macrophages in response to apoptotic cells requires activation of the scavenger receptor CD36. PLoS ONE *8*, e72772.

Yoshida, S., Gaeta, I., Pacitto, R., Krienke, L., Alge, O., Gregorka, B., and Swanson, J.A. (2015). Differential signaling during macropinocytosis in response to M-CSF and PMA in macrophages. Front. Physiol. *6*, 8.

Yurdagul, A., Jr., Subramanian, M., Wang, X., Crown, S.B., Ilkayeva, O.R., Darville, L., Kolluru, G.K., Rymond, C.C., Gerlach, B.D., Zheng, Z., et al. (2020). Macrophage metabolism of apoptotic cell-derived arginine promotes continual efferocytosis and resolution of injury. Cell Metab. *31*, 518–533.e10.

Zhang, S., Weinberg, S., DeBerge, M., Gainullina, A., Schipma, M., Kinchen, J.M., Ben-Sahra, I., Gius, D.R., Yvan-Charvet, L., Chandel, N.S., et al. (2019). Efferocytosis fuels requirements of fatty acid oxidation and the electron transport chain to polarize macrophages for tissue repair. Cell Metab. *29*, 443–456.e5.

Zheng, B., Mao, J.H., Li, X.Q., Qian, L., Zhu, H., Gu, D.H., and Pan, X.D. (2016). Over-expression of DNA-PKcs in renal cell carcinoma regulates mTORC2 activation, HIF-2α expression and cell proliferation. Sci. Rep. *6*, 29415.

STAR★METHODS

KEY RESOURCES TABLE

REAGENT or RESOURCE	SOURCE	IDENTIFIER
Antibodies		
Rabbit anti-p-Akt (S473)	Cell Signaling Technology	Cat# 4060S; RRID: AB_2315049 (1:2000 dilution)
Rabbit anti-Akt	Cell Signaling Technology	Cat# 4691S; RRID: AB_915783 (1:2000 dilution)
Rabbit anti-Rictor	Cell Signaling Technology	Cat# 2114S; RRID: AB_2179963 (1:2000 dilution)
Rat anti-Mac2	Cedarlane	Cat# CL8942AP; RRID:AB_10060357 (1:10,000 dilution)
Rabbit anti-c-Myc	Proteintech	Cat# 10828-1-AP; RRID: AB_2148585 (1:200 dilution)
Rabbit anti-β-actin-HRP	Cell Signaling Technology	Cat# 5125S; RRID: AB_1903890 (1:5000 dilution)
Mouse anti-c-Myc	Invitrogen	Cat# MA1-980; RRID: AB_558470 (1:200 dilution)
Rabbit anti-c-Myc	Cell Signaling Technology	Cat# 18583S; (1:2500 dilution)
Rabbit anti-DNA-PKcs	Invitrogen	Cat# MA5-32192; RRID: AB_2809479 (1:200 dilution)
Rabbit anti-Bhlhe40	Invitrogen	Cat# PA1-16546; RRID: AB_2065348 (1:200 dilution)
Rabbit anti-cMaf	Invitrogen	Cat# PA5-23179 RRID: AB_2540705 (1:200 dilution)
Rabbit anti-Ki67	Abcam	Cat# ab16667; RRID: AB_302459 (1:200 dilution)
Sheep anti-Ki67	R&D Systems	Cat# AF7649; RRID: AB_2687500 (1:200 dilution)
Rabbit anti-Irf4	Invitrogen	Cat# 11247-2-AP; RRID: AB_2264940(1:200 dilution)
Rabbit anti-Alox15	Bioss	Cat# bs-6505R; RRID: AB_11051537(1:200 dilution)
Rabbit anti-Phospho-p44/42 MAPK (Erk1/2) (Thr202/Tyr204)	Cell Signaling Technology	Cat# 4370S; RRID: AB_2315112 (1:200 dilution)
Rat anti-mouse F4/80 (PE/Cy7)	Biolegend	Cat# 123113; RRID:AB_893490 (1:100 dilution)
Rat anti-mouse IL-10 (PE)	Invitrogen	Cat# 12-7101-41 RRID: AB_10669561 (1:100 dilution)
Rabbit anti-Cxcl10/IP-10	Thermo Fisher Scientific	Cat# MA5-32674; RRID:AB_2809951 (1:100 dilution)
Goat anti-IL-6	R&D Systems	Cat# AF-406-NA RRID:AB_354478 (1:200 dilution)
Rabbit anti-phospho-DNA-PKcs (Thr 2609)	Invitrogen	Cat# PA5-105749 RRID:AB_2817148 (1:200 dilution)
Rabbit anti-Rictor	Novus	Cat# NB100-612 RRID:AB_10000886
APC anti-mouse LAP (TGF-β1)	Biolegend	Cat# 141406 RRID: AB_10898159 (1:100 dilution)
APC anti-mouse Ly-6G/Ly-6C (Gr-1)	Biolegend	Cat# 108412 RRID: AB_313377 (1:100 dilution)
Rabbit IgG	Sigma-Aldrich	Cat# PP64B; RRID:AB_97852
Goat anti-mouse (HRP)	Invitrogen	Cat# 32230; RRID:AB_1965958 (1:2000 dilution)
Goat anti-rabbit (HRP)	Invitrogen	Cat# 32260; RRID:AB_1965959 (1:2000 dilution)
Goat anti-mouse (AF488)	Invitrogen	Cat# A11001; RRID:AB_2534069 (1:200 dilution)
Goat anti-mouse (AF555)	Invitrogen	Cat# A28180; RRID:AB_2536164 (1:200 dilution)
Goat anti-rat (AF488)	Invitrogen	Cat# A11006; RRID:AB_141373 (1:200 dilution)
Goat anti-rabbit (AF488)	Invitrogen	Cat# A11034; RRID:AB_2576217 (1:200 dilution)
Goat anti-rabbit (AF555)	Invitrogen	Cat# A21428; RRID:AB_141784 (1:200 dilution)
Chicken anti-rabbit (AF647)	Invitrogen	Cat# A-21443 RRID: AB_2535861 (1:200 dilution)
Goat anti-Rat (AF647)	Invitrogen	Cat# A21247; RRID:AB_141778 (1:200 dilution)
Pacific Blue anti-F4/80	Biolegend	Cat# 123123; RRID:AB_893487 (1:100 dilution)

(*Continued on next page*)

Continued

REAGENT or RESOURCE	SOURCE	IDENTIFIER
Chemicals, peptides, and recombinant proteins		
Dulbecco's Modified Eagle Media (DMEM)	Corning	Cat# 10-013-CV
Roswell Park Memorial Institute (RPMI) 1640 Media	Corning	Cat# 10-040-CV
Opti-MEM	GIBCO	Cat# 31985-070
1X HBSS	Corning	Cat# 21-022-CV
1X PBS	Corning	Cat# 21-040-CV
CellStripper	Corning	Cat# 25-056-CI
Heat-Inactivated Fetal Bovine Serum	GIBCO	Cat# 10438-026
Penicillin/Streptomycin	Corning	Cat# 30-002-CI
Human Macrophage Colony Stimulating Factor (M-CSF)	Peprotech	Cat# 300-25
HISTOPAQUE-1077	Sigma-Aldrich	Cat# 10771-100ML
2-Well Glass Slides	Thermo Scientific	Cat# 155380
4-Well Glass Slides	Thermo Scientific	Cat# 155383
8-Well Glass Slides	Thermo Scientific	Cat# 155411
Novex 4-20% Tris-Glycine Mini Gels, 15-well	Invitrogen	Cat# XP04205BOX
2X Laemmli Buffer	Bio-Rad	Cat# 1610747
PKH67 Fluorescent Cell Linker	Sigma-Aldrich	Cat# PKH67GL-1KT
PKH26 Fluorescent Cell Linker	Sigma-Aldrich	Cat# PKH26GL-1KT
Cell-Vue Claret Fluorescent Cell Linker	Sigma-Aldrich	Cat# MINCLARET-1KT
Diluent C	Sigma-Aldrich	Cat# CGLDIL
Interleukin-4	Sigma-Aldrich	Cat# SRP3211
Interferon-γ (IFN-γ)	Peprotech	Cat# 315-05
Cytochalasin D	Sigma-Aldrich	Cat# C8273
U0126	Tocris Bio-Techne	Cat# 1144
DMSO	Sigma-Aldrich	Cat# D2650
β-mercaptoethanol	Bio-Rad	Cat# 1610710
Citrate-dextrose solution	Sigma-Aldrich	Cat# C3821
Recombinant mouse Gas6 protein	R&D Systems	Cat# 986-GS
pHrodo Green	Thermo Scientific	Cat# P35373
pHrodo Red	Thermo Scientific	Cat# P35372
CMLD-2	Sigma-Aldrich	Cat# 538339
Recombinant HuR	Novus Biologicals	Cat# H00001994-P01
Bafilomycin A1	Sigma-Aldrich	Cat# B1793
Dexamethasone	Calbiochem	Cat# 265005
Actinomycin D	Sigma-Aldrich	Cat# A1410
Annexin V (FITC)	BD Biosciences	Cat# 560931
Zymosan A	Sigma-Aldrich	Cat# Z4250
Lipofectamine RNAiMax	Life Technologies	Cat# 13778-150
Neomycin	Sigma-Aldrich	Cat# N1142
Polymyxin B	Sigma-Aldrich	Cat# P4932
40 μm Nylon Cell Strainers	BD Falcon	Cat# 352340
Power SYBR Green PCR Master Mix	Applied Biosystems	Cat# 4367659
EdU Proliferation Assay Kit	Abcam	Cat# ab219801
AFDye 488 Azide	Click Chemistry Tools	Cat# 1275-1
AFDye 555 Azide	Click Chemistry Tools	Cat# 1287-1
Copper (II) Sulfate Solution	Sigma-Aldrich	Cat# C2284-25ML

(*Continued on next page*)

Continued

REAGENT or RESOURCE	SOURCE	IDENTIFIER
(+)-Sodium L-Ascorbate	Sigma-Aldrich	Cat# A4034-100G
BD BD GolgiStop	Thermo Scientific	Cat# BDB554724
50:50 PLGA (inherent viscosity range of 0.55 to 0.75 dl/g, 43.4 kDa)	LACTEL Absorbable Polymers by DURECT Corporation	Cat# B6013-2
DSPE-PEG (MW, 3 kDa)	Avanti Polar Lipids	Cat# 880320
DSPE-PEG-Mal (PEG molecular weight, 3.4 kDa)	Nanocs Inc.	Cat# PG2-DSML-3k
S2P peptide (CRTLTVRKC)	GLS Biochem Systems Inc	Cat# 652358
ethylenediamine core-poly (amidoamine) (PAMAM) generation 0 dendrimer	Sigma-Aldrich	Cat# 412368
1,2-epoxytetradecane	Sigma-Aldrich	Cat# 260266
0.45-mm nitrocellulose membranes	Bio-Rad	Cat# 1620115
Hoechst 33342	Thermo Scientific	Cat# 62249
Lipofectamine RNAiMax	Life Technologies	Cat# 13778-150
Perm buffer II	BD Biosciences	Cat# 558052
Critical commercial assays		
PureLink RNA Mini Kit	Thermo Fisher Scientific	Cat# 12183025
TUNEL Kit	Roche	Cat# 12156792910
Supersignal West Pico Chemiluminescence Kit	Thermo Fisher Scientific	Cat# 34080
Total Cholesterol Kit	Wako Diagnostics	Cat# 999-02601
Experimental models: Cell lines		
Human: Jurkat cells	ATCC	ATCC TIB-152
Mouse: L-929 Fibroblast cells	ATCC	ATCC CCL-1
Mouse: Bone Marrow-Derived Macrophage cells	This paper	N/A
Mouse: Elicited Peritoneal Macrophage cells	This paper	N/A
Human: Peripheral Blood Monocyte-Derived Macrophage cells	This paper	N/A
Sheep Red Blood Cells 10% washed pooled cells	Rockland Immunochemicals, Inc.	R405-0050
Experimental models: Organisms/strains		
Mouse: C57BL/6J	The Jackson Laboratory	JAX: 000664
Mouse: $Ldlr^{-/-}$: C57BL/6J	The Jackson Laboratory	JAX: 002207
Mouse: $Rictor^{fl/fl}$:C57BL/6J	The Jackson Laboratory	JAX: 020649
Mouse: Lyz2cre: C57BL/6J	Cai et al., 2020	N/A
Mouse: $MerTK^{fl/fl}$: C57BL/6J	Fourgeaud et al., 2016	N/A
Oligonucleotides		
ON-TARGETplus non-targeting pool	GE Healthcare Dharmacon	D-001810-10-05
Mouse: ON-TARGETplus Rubicon siRNA	GE Healthcare Dharmacon	L-172564-00-0005
Mouse: IDT DNase2a DsiRNA	Integrated DNA Technologies	mm.Ri.Dnase2a.13.1
Mouse: IDT Rictor DsiRNA	Integrated DNA Technologies	mm.Ri.Rictor.13.1
Mouse: IDT PRKDC DsiRNA	Integrated DNA Technologies	mm.Ri.Prkdc.13.1
Mouse: IDT Bhlhe40 DsiRNA	Integrated DNA Technologies	mm.Ri.Bhlhe40.13.1
siScramble sense: 5′-CUUACGCUGAGUACUUCGATT-3′, antisense: 5′-UCGAAGUACUCAGCGUAAGTT-3′	Horizon Discovery Ltd.	N/A
Mouse: cMyc siRNA	Sigma-Aldrich	SASI_Mm01_00157474
Mouse: *DNase2a* Forward AAGCCCTGAGCTGCTATGG	PrimerBank	https://pga.mgh.harvard.edu/primerbank/index.html

(*Continued on next page*)

Continued

REAGENT or RESOURCE	SOURCE	IDENTIFIER
Mouse: *DNase2a* Reverse ATACGTCAGTCCCTTTGGAGTA	PrimerBank	https://pga.mgh.harvard.edu/primerbank/index.html
Mouse: *Hprt* Forward TCAGTCAACGGGGGACATAAA	PrimerBank	https://pga.mgh.harvard.edu/primerbank/index.html
Mouse: *Hprt* Reverse GGGGCTGTACTGCTTAACCAG	PrimerBank	https://pga.mgh.harvard.edu/primerbank/index.html
Mouse: *Rictor* Forward ACAGTTGGAAAAGTGGCACAA	PrimerBank	https://pga.mgh.harvard.edu/primerbank/index.html
Mouse: *Rictor* Reverse GCGACGAACGTAGTTATCACCA	PrimerBank	https://pga.mgh.harvard.edu/primerbank/index.html
Mouse: *Prkdc* Forward AAACCTGTTCCGAGCTTTTCTG	PrimerBank	https://pga.mgh.harvard.edu/primerbank/index.html
Mouse: *Prkdc* Reverse TCTCAATCTGAGGACGAATTGC	PrimerBank	https://pga.mgh.harvard.edu/primerbank/index.html
Mouse: *Rbcn* Forward CAGGGTGTAGTGCATGGTTCT	PrimerBank	https://pga.mgh.harvard.edu/primerbank/index.html
Mouse: *Rbcn* Reverse CCGCCAAGATCCATTCCCG	PrimerBank	https://pga.mgh.harvard.edu/primerbank/index.html
Mouse: *Bhlhe40* Forward ACGGAGACCTGTCAGGGATG	PrimerBank	https://pga.mgh.harvard.edu/primerbank/index.html
Mouse: *Bhlhe40* Reverse GGCAGTTTGTAAGTTTCCTTGC	PrimerBank	https://pga.mgh.harvard.edu/primerbank/index.html
Mouse: *Maf* Forward GGAGACCGACCGCATCATC	PrimerBank	https://pga.mgh.harvard.edu/primerbank/index.html
Mouse: *Maf* Reverse TCATCCAGTAGTAGTCTTCCAGG	PrimerBank	https://pga.mgh.harvard.edu/primerbank/index.html
Mouse: *Myc* Forward TGACCTAACTCGAGGAGGAGCTGGAA	PrimerBank	https://pga.mgh.harvard.edu/primerbank/index.html
Mouse: *Myc* Reverse AAGTTTGAGGCAGTTAAAATTATGGCT	PrimerBank	https://pga.mgh.harvard.edu/primerbank/index.html
Mouse: *G6pdx* Forward CACAGTGGACGACATCCGAAA	PrimerBank	https://pga.mgh.harvard.edu/primerbank/index.html
Mouse: *G6pdx* Reverse AGCTACATAGGAATTACGGGCAA	PrimerBank	https://pga.mgh.harvard.edu/primerbank/index.html
Mouse: *DNase1* Forward CTCAATCGGTGGGTGACAGTA	PrimerBank	https://pga.mgh.harvard.edu/primerbank/index.html
Mouse: *DNase1* Reverse TGTCCCTGGATAAAGGAAACCA	PrimerBank	https://pga.mgh.harvard.edu/primerbank/index.html
Recombinant DNA		
cMaf Rat tagged ORF cDNA expression plasmid	Origene	Cat# RR209464
HDAd-LDLR	Baylor College of Medicine	Willecke et. al., 2015
Software and algorithms		
NIS-Elements	Nikon	Advanced Research
Leica Application Suite	Leica	Advanced Fluorescence
Imaris 9.5.0	Oxford Systems	N/A
ImageJ	NIH	https://imagej.nih.gov/ij/
FIJI	NIH	https://fiji.sc/
PRISM	GraphPad Software	Version 6
FlowJo	FlowJo, LLC	Version 10

(*Continued on next page*)

Continued

REAGENT or RESOURCE	SOURCE	IDENTIFIER
Other		
Genotyping Service	Genetyper	https://www.genetyper.com/
Salmon Sperm DNA Ready-to-Use Solution	Rockland Immunochemicals, Inc.	MB-103-0025
Mouse Diet: High-Fat Western Diet	Envigo	Cat# TD.88137
Helper-Dependent Adenovirus Cloning and Packaging Services	Baylor College of Medicine	N/A

RESOURCE AVAILABILITY

Lead contact

Further information and requests for resources and reagents should be directed to and will be fulfilled by the lead contact, Dr. Ira Tabas (iat1@cumc.columbia.edu).

Materials availability

This study did not generate new unique reagents.

Data and code availability

- All data reported in this paper will be shared by the lead contact upon request.
- This paper does not report original code.
- Any additional information required to reanalyze the data reported in this paper is available from the lead contact upon request

EXPERIMENTAL MODEL AND SUBJECT DETAILS

Cell lines

Jurkat (human T lymphocytes) and L-929 (mouse fibroblasts) cells were obtained from ATCC and cultured in DMEM (GIBCO) supplemented with 10% (vol/vol) heat-inactivated fetal bovine serum (HI-FBS; GIBCO), 10 U/mL penicillin, and 100 mg/mL streptomycin (Corning). Cells were cultured in 5% CO_2 incubator at 37°C.

Primary cell culture

To culture bone marrow-derived macrophages (BMDMs), bone marrow was isolated from 8-12 week old mice (male) and cultured for 7-10 days in DMEM supplemented with 10% heat-inactivated fetal bovine serum (HI-FBS), 10 U/mL penicillin, 100 mg/mL streptomycin and 20% L-929 fibroblast-conditioned media (L-cell conditioned media). To elicit a pro-resolving macrophage phenotype, BMDMs were incubated with 10 ng/mL recombinant mouse IL-4 (Sigma-Aldrich) for 24 h. To elicit a pro-inflammatory macrophage phenotype, BMDMs were incubated with 50 ng/mL LPS + 25 ng/mL IFNγ (Peprotech) for 24 h. Cells were cultured in 5% CO2 incubator at 37°C

Human samples

Human macrophages were derived from peripheral human blood monocytes that were isolated from buffy coats, purchased from the New York Blood Center, of anonymous, de-identified healthy adult volunteers, with informed consent. University Institutional Review Board and Health Insurance Portability and Accountability Act guidelines were followed. Monocytes were isolated in a discontinuous gradient of Histopaque solution. After 4 h of adhesion on 24-well plates, cells were rinsed, and medium was changed to RPMI-1640 (GIBCO) containing 10% HI-FBS, 10 U/mL penicillin and 100 mg/mL streptomycin, and 10 ng/mL of M-CSF (Peprotech). These cells were then used for experiments after 7-10 days when they were more than 75% confluent. Cells were cultured in 5% CO_2 incubator at 37°C.

Mouse studies

Animal protocols were approved by Columbia University's institutional animal care and use committee. All mice were cared for according to the NIH guidelines for the care and use of laboratory animals, and were in good general health based on appearance and activity. The mice were housed in standard cages at 22°C under a 12-12 h light-dark cycle in a barrier facility with *ad libitum* access to water and food. *Mertk*$^{fl/fl}$ *Lyz2cre* male mice on the C57BL/6J background were generated as previously described (Cai et al., 2020; Fourgeaud et al., 2016). Male wild-type C57BL/6J and *Rictor*$^{fl/fl}$ mice (8-10 weeks/old) were obtained from Jackson Laboratory (Bar Harbor, ME) and were allowed to adapt to housing conditions in animal facility for 1 week before commencement of experiments. Littermate control mice were randomly assigned to experimental groups by investigators. Investigators were blinded for the atherosclerosis studies but were not blinded for the zymosan-induced sterile peritonitis or the dexamethasone-induced thymus injury experiments.

METHOD DETAILS

Induction of apoptosis and fluorescent labeling of Jurkat cells

Jurkat cells were irradiated with 254-nm UV lamp for 15 min, followed by incubation at 37°C 5% CO_2 for 2-3 h. This method typically generates 85% annexin-V^+ cells. The apoptotic cells (ACs) were resuspended in 1x PBS at a concentration of 2 $X10^7$ cells/mL with 5 μL of Vybrant® DiD cell-labeling solution (Invitrogen) for 10 min. For efferocytosis assays involving the sequential uptake of differentially labeled ACs added at 2 different times, ACs were suspended at the same concentration, but in Diluent C (Sigma-Aldrich), and incubated for 5 min with 4 mL of Diluent C containing concentrated PKH67 or PKH26 membrane-intercalating dyes (Sigma-Aldrich). Cells were rinsed twice with 1x PBS and resuspended at a concentration 4 X 10^6 cells/mL in DMEM containing 10% heat-inactivated FBS, and then used for experiments.

siRNA-mediated gene silencing

Scrambled RNA control and oligo-targeted siRNAs were transfected into macrophages in 24-well plates using Lipofectamine RNAiMAX (Life Technologies) using 50 nM of siRNA per well. After 18 h, the media were changed to DMEM/10% FBS, and the cells were incubated for an additional 30 h.

Efferocytosis-induced macrophage proliferation assay and flow cytometry

BMDMs were incubated with 20 μM of EdU solution (Abcam) for 1 h prior to the addition of DiD-labeled apoptotic Jurkat cells for 45min. After 45 min, the macrophages were rinsed with PBS to remove unbound ACs and incubated for 24 h in DMEM containing 10% heat-inactivated FBS. After 24 h, the macrophages were detached using Cell Stripper (Invitrogen), pelleted by centrifugation at 3000 x g for 3 min, resuspended in FACS-staining buffer (PBS containing 2% FBS and 1 mM EDTA) at a density of 1 X 10^6 in 200 μL, and incubated on ice with Fc Receptor Blocking Solution (anti-mouse CD16/32; Biolegend) for 30 min. The macrophages were then pelleted by centrifugation and resuspended in 4% paraformaldehyde. After 15 min, the cells were rinsed, suspended in permeabilization buffer containing 0.1% saponin, and immunostained with fluorescent-labeled antibodies for 60 min on ice. The macrophages were then washed with permeabilization buffer, and EdU staining was carried out using the Abcam EdU Proliferation Kit (iFluor 488) at room temperature. The macrophages were then suspended in flow tubes and analyzed on a BD FACS Canto II flow cytometer. Data analysis was carried out using FlowJo software. For other flow cytometric experiments, non-permeabilized and saponin-permeabilized macrophages were incubated with fluorescent antibodies for 60 min on ice to label cell-surface and intracellular proteins, respectively. in other experiments, the macrophages were first incubated with unlabeled primary antibodies for 2 h, rinsed three times with FACS buffer containing 0.1% saponin, and incubated with fluorescently-conjugated secondary antibodies for an additional 2 h. The cells were then subjected to flow cytometric analysis as above.

Cell number counting

Bone marrow-derived macrophages were incubated in the presence or absence of unlabeled ACs for 45 min at a 5:1 AC:macrophage ratio. The wells were then rinsed with PBS to remove unengulfed ACs, and the macrophages were incubated for an additional 24 h, after which they were detached using Cell Stripper (Invitrogen) and counted using the Countess II Automated Cell Counter (Invitrogen).

CFSE proliferation assay

Macrophages were incubated with 5(6)-Carboxyfluorescein diacetate N-hydroxysuccinimidyl ester (CFSE) for 15 min, then washed with DMEM to remove non-incorporated dye. The cells were then incubated with DiD-labeled ACs for 45 min, followed by rinsing and incubation for an additional 24 h. The macrophages were then removed from the dish, fixed with 4% PFA, resuspended in FACS buffer, and subjected to assay of CFSE fluorescence by flow cytometry. Data analysis was carried out using FlowJo software.

Assay of single-AC and sequential double-AC uptake by control macrophages and EIMP-induced proliferative macrophages

For EIMP-induced proliferative macrophages, BMDMs were plated in 24-well plates at a density of 1.8 X 10^5 cells per well and incubated with unlabeled ACs for 45 min at a 5:1 AC:macrophage ratio. The wells were rinsed with PBS to remove unengulfed ACs, and the macrophages were incubated in culture medium for 24 h. The cells were then incubated with PKH67-labeled ACs for 45 min at a 5:1 AC:macrophage ratio, followed by rinsing with PBS. One cohort was harvested for analysis (single-AC efferocytosis), while a second cohort was incubated for another 2 h in normal cell culture media, followed by the addition of PKH27-labeled ACs (double-AC efferocytosis). After 45 min, the monolayers were rinsed with PBS, and then the macrophages were fixed with 4% paraformaldehyde for 15 min, rinsed with PBS, permeabilized with Triton X-100, and immunostained using anti-Ki67. For control macrophages, the initial 24 h incubation with unlabeled ACs was omitted. The macrophages were imaged on a Leica epifluorescence microscope (DMI6000B), and the images were analyzed using Imaris 9.5 quantification software for $Ki67^-$ and $Ki67^+$ macrophages containing PKH67 alone or both PKH67 and PKH27.

Nuclear EdU incorporation assay

Live Jurkat cells were incubated with 20 μM EdU (Abcam) for 2 h, washed three times with PBS, labeled with DiD cell membrane-labeling solution, and then rendered apoptotic as above. Macrophages were then incubated with the EdU-labeled ACs for

45mins, followed by washing twice with PBS and then incubation for 18 h. The cells were then fixed with 4% PFA, macrophage nuclei were counterstained with DAPI, and images were taken on a Leica epifluorescence microscope (DMI6000B). Image analysis was conducted using Imaris 9.5 quantification software to quantify the percentage of macrophages with nuclear EdU staining not associated with DiD^+ AC material.

Assay of TGFβ and IL-10 by EIMP-induced proliferative macrophages

BMDMs were plated in 24-well plates at a density of 1.8×10^5 cells per well and incubated with EdU for 1 h prior to the addition of DiD-labeled ACs at a 5:1 AC:macrophage ratio. After 45 min, the macrophages were rinsed with PBS and incubated overnight in DMEM containing 10% FBS and 2 μL/mL Protein Transport Inhibitor Cocktail (eBioscience; Invitrogen) to prevent exosomal release of secreted proteins. The macrophages were then rinsed, detached, pelleted by centrifugation, resuspended in FACS buffer containing Fc receptor blocker, and incubated for 30 min. Cells were then pelleted and resuspended in 4% paraformaldehyde for 15 min, followed by permeabilization with 0.1% saponin. Intracellular staining was carried out with fluorescent antibodies against TGFβ and IL-10 for 60 min on ice. The cells were then rinsed with permeabilization buffer, stained at room temperature with EdU using the Abcam EdU Proliferation Kit (iFluor 488), resuspended in FACS buffer, and analyzed on a BD FACS Canto II flow cytometer. Data analysis was carried out using FlowJo software.

Zymosan-induced peritonitis and peritoneal uptake of labeled ACs

EdU (200 μg/mouse) was injected i.p., and 24 h later sterile peritonitis was induced by a single 500 μL i.p. injection of 1 mg zymosan A (Sigma-Aldrich). After 24 or 48 h, the mice were euthanized, and peritoneal lavage fluid was collected with using 3 mL of PBS. The lavage fluid was passed through a 40-μm strainer and the cells were pelleted by centrifugation and resuspended in FACS buffer containing Fc receptor blocker. After 30 min incubation on ice, the cells were incubated for 2 h with fluorescently conjugated anti-F4/80 antibody (BioLegend). The cells were washed with then FACs buffer three times and suspended in permeabilization buffer containing anti-Ly-6G/Ly-6C (Gr-1) (Biolegend) to stain engulfed apoptotic neutrophils. After incubation overnight. To distinguish between external and internalized neutrophils in the macrophages, cell-surface staining with anti-F4/80 and anti-Gr-1 of non-permeabilized cells was used. After an overnight incubation, the cells were stained at room temperature for EdU using the Abcam EdU Proliferation Kit (iFluor 488). The cells were then washed twice and resuspended in FACs buffer and placed into flow tubes for analysis on a BD FACs Cantos II flow cytometer. Data analysis was carried out using FlowJo software.

Bone marrow transplant

Eight-week old male C57BL/6J mice were irradiated using 1,000 rads from a 137 Cesium GammaCell source. The same day, bone marrow cells were harvested from a *Rictor*$^{fl/fl}$ mouse and incubated with 5 μM of TAT-CRE Recombinase (Millipore) for 30 min to delete the floxed *Rictor* gene or vehicle control. The Rictor-deleted control bone marrow cells were then rinsed twice with PBS, resuspended at 2.5×10^6 cells, and injected via tail vein into the irradiated C57BL/6J recipient mice. Recipient mice were given acidic water containing 10 mg/mL neomycin for 3 weeks following the bone marrow transplant. After 4 weeks, the thymus efferocytosis assay described below was conducted.

Thymus assays

Mice transplanted with control or Rictor-deleted bone marrow were injected i.p. with 250 μL PBS containing 250 μg dexamethasone (Sigma-Aldrich) dissolved in DMSO. Eighteen h after injection, the mice were euthanized, and thymi were harvested and weighed. One lobe of the thymus was mechanically dissociated, and cells were counted to determine total cell number. Cells were then stained with annexin-V and anti-F4/80, followed by flow cytometry to determine the number of thymic ACs and macrophages. The other lobe of the thymus was fixed in 4% paraformaldehyde, paraffin-embedded, and sectioned, followed by staining of 5-μm sections with TUNEL reagent (Roche), anti-Mac2 (Cedarlane), anti-Ki67 (Abcam), and anti-c-Myc (ThermoFisher), anti-Bhlhe40 (ThermoFisher), and anti-c-Maf (ThermoFisher). Fluorescence microscopic imaging was use to quantify $Mac2^+$ $Ki67^+$ macrophages with cytoplasmic TUNEL ($cTUN^+$), indicative of proliferation in efferocytic macrophages. Also, efferocytosis was assessed by quantifying the ratio $cTUN^+$ cells associated with $Mac2^+$ macrophages to non-macrophage-associated ("free') $cTUN^+$ cells.

siRictor and siDnase2a S2P-nanoparticles

50:50 PLGA, with inherent viscosity range of 0.55 to 0.75 dl/g and size of 43.4 kDa, was purchased from LACTEL Absorbable Polymers by DURECT Corporation (catalog # B6013-2). DSPE-PEG (3 kDa) was obtained from Avanti Polar Lipids (catalog # 880320), and DSPE-PEG-Mal (PEG molecular weight 3.4 kDa) was purchased from Nanocs Inc. (catalog # PG2-DSML-3k). CRTLTVRKC peptide was from GLS Biochem Systems Inc (catalog # 652358). The cationic lipid G0-C14 and targeted lipid-PEG (DSPE-PEG-S2P) were synthesized according to our previous reports (Kamaly et al., 2013; Tao et al., 2020). Using siRictor and siDnase2a, the targeted siRNA-loaded S2P50 NPs were then prepared using an optimized nano-precipitation method modified from our previous report (Tao et al., 2020). Specifically, the interaction time between G0-C14 and siRNAs was increased from 10 s to 30 s, together with gentle, repeated mixing with a pipette, to enhance more effective complexation; and the magnetic stirring rpm was increased from 1000 to 1200, and the preparation time was increased from 1 h to 1.5 h, to enable more effective volatilization of organic solvent. All procedures were conducted under aseptic conditions to avoid contamination.

Tissue collection and lesion analysis

Ten-week-old male *Ldlr*$^{-/-}$ mice were placed on Western diet (Envigo, TD 88137) for a total of 16 weeks. One cohort was harvested at that time (baseline), and other cohorts (regression) were injected with a helper-dependent adenovirus containing the human *Ldlr* gene (HDAd-LDLR) and simultaneously placed a chow diet for an additional five weeks. This virus is a non-integrating vector that primarily targets the liver and restores expression of the *Ldlr* in hepatocytes to levels sufficient to markedly reduce circulating cholesterol in *Ldlr*$^{-/-}$ mice. For the regression cohorts, the mice were administered S2P-nanoparticles containing control scrambled RNA (Scr), siRictor, or siDnase2a at the start of the regression period. The nanoparticles were administered twice a week during the five-week regression period. Upon sacrifice, mice were perfused with PBS through left ventricular cardiac puncture, and aortic roots were collected and processed for histology. Sections were stained with hematoxylin and eosin for morphometric lesion analysis. Atherosclerotic lesion area, defined as the space from the internal elastic lamina to the lumen, was quantified by taking the average of 6 sections spaced 30-μm apart, beginning at the base of the aortic root. Boundary lines were drawn around these regions, and the area measurements were obtained by image analysis software. A 3,000-μm^2 threshold cut-off was applied to acellular regions to calculate areas of necrosis. Thickness of the collagen-rich fibrous cap was assessed in picrosirius red-stained sections, with the width of the cap measured at the lesional midpoint and both shoulder regions and then averaged and quantified as the ratio of mean collagen cap thickness to lesion area. Fasting blood glucose levels were measured using ONETOUCH Ultra after food was withdrawn for 18 h. Total plasma cholesterol was measured using a WAKO Diagnostics kit. Complete blood cell counts, including leukocyte differential, were obtained using a FORCYTE Hematology Analyzer (Oxford Science).

Tissue immunohistochemistry and immunofluorescence microscopy

Paraffin-embedded specimens were sectioned, de-paraffinized with xylene, and rehydrated in decreasing concentrations of ethanol. Antigen retrieval and unmasking were achieved by incubation with citrate buffer (1:100 dilution), followed by pressure cooking for 10 min. After cooling, the sections were incubated with TUNEL reagent for 60 min at 37°C and washed 3 times with PBS. The sections were then incubated for 60 min with blocking solution, consisting of PBS containing 2% bovine serum albumin (BSA). The sections were then incubated overnight at 4°C with anti-Mac2 (1:10,000), anti-Ki67 (1:200), anti-Myc (1:200), anti-Bhlhe40 (1:200), anti-c-Maf (1:200), anti-Rictor (1:100), anti-MerTK (1:200), anti-Arg1 (1:200), anti-IL-6 (1:100), anti-CXCL10 (1:100), anti-IRF4 (1:200), anti-ALOX15 (1:200), and anti-SR-BI (1:200) antibodies. On the following day, the sections were washed in PBS and incubated with fluorescently-labeled secondary antibodies for 2 h, washed, dried, and counterstained with DAPI. Images were taken using a Leica epi-fluorescence microscope (DMI6000B) or, for spinning disk confocal microscopy, a Nikon Ti Eclipse inverted microscope. Image analysis was completed using Imaris 9.5 quantification software.

Immunoblotting

BMDMs were lysed in 2X Laemmli lysis buffer (Bio-Rad) containing 50 mM β-mercaptoethanol. The cell lysates were heated at 95°C for 10-15 min, separated on 4%–20% SDS-PAGE gradient gels (Invitrogen) at 150 V for 1.5 h, and electro-transferred to nitrocellulose membranes at 100V for 2-3 h. For larger proteins, such as Rictor (250kDa), electro-transfer to nitrocellulose membranes was carried out overnight at 23V. The membranes were incubated with 5% milk for 1 h followed by rinsing in Tri-buffered saline containing Tween-20 (TBST) and incubation overnight at 4°C with primary antibodies in PBS containing 1% BSA. Primary antibodies were detected with using HRP-conjugated secondary antibodies (Pierce). Densitometry was performed using ImageJ software.

Quantitative real time PCR

RNA was extracted from BMDMs using the PureLink RNA Mini kit (Thermo Fisher Scientific). The quality and concentration of RNA was determined by absorbance at 260 and 280nm using a NanoDrop spectrophotometer (Thermo Fisher Scientific). Complementary DNA was synthesized from 0.5-1 μg of RNA, which had a 260/280 ratio of > 1.8, using oligo (dT) and Superscript II (Applied Biosystems). Quantitative RT-PCR was performed using a 7500 Real-Time PCR system (Applied Biosystems) and SYBR Green Master Mix reagents (Applied Biosystems).

Electroporation of overexpression plasmids

Macrophages were transfected with Maf1 plasmid via electroporation (Invitrogen). *Maf* plasmid DNA at (0.75 μg) was added directly to 5 X 10^5 pelleted macrophages. Cells and DNA were resuspended in 150 μL of R-buffer (Invitrogen) and subjected to electroporation at 1550 mV with 10 ms intervals for 2 pulses. The macrophages were then plated directly into 24-well plates and experiments were conducted two days later.

QUANTIFICATION AND STATISTICAL ANALYSIS

Data were tested for normality using either the D'Agostino-Pearson or Shapiro-Wilk test, and statistical significance was determined using GraphPad Prism software. *P*-values for normally distributed data were calculated using either the Student's t test for two groups or one-way ANOVA with Fisher's Least Significant Difference (LSD) post hoc analysis when there were three or more groups. *P*-values for non-normally distributed data were calculated using the Mann-Whitney rank sum test or the uncorrected Dunn's test. Data are shown as mean values ± SEM. Graphical representation of differences that are statistically significant at p £ 0.05 are signified by different letters. Data marked by the same letter are not statistically significant.

Cell Metabolism, Volume *33*

Supplemental information

Efferocytosis induces macrophage proliferation to help resolve tissue injury

Brennan D. Gerlach, Patrick B. Ampomah, Arif Yurdagul Jr., Chuang Liu, Max C. Lauring, Xiaobo Wang, Canan Kasikara, Na Kong, Jinjun Shi, Wei Tao, and Ira Tabas

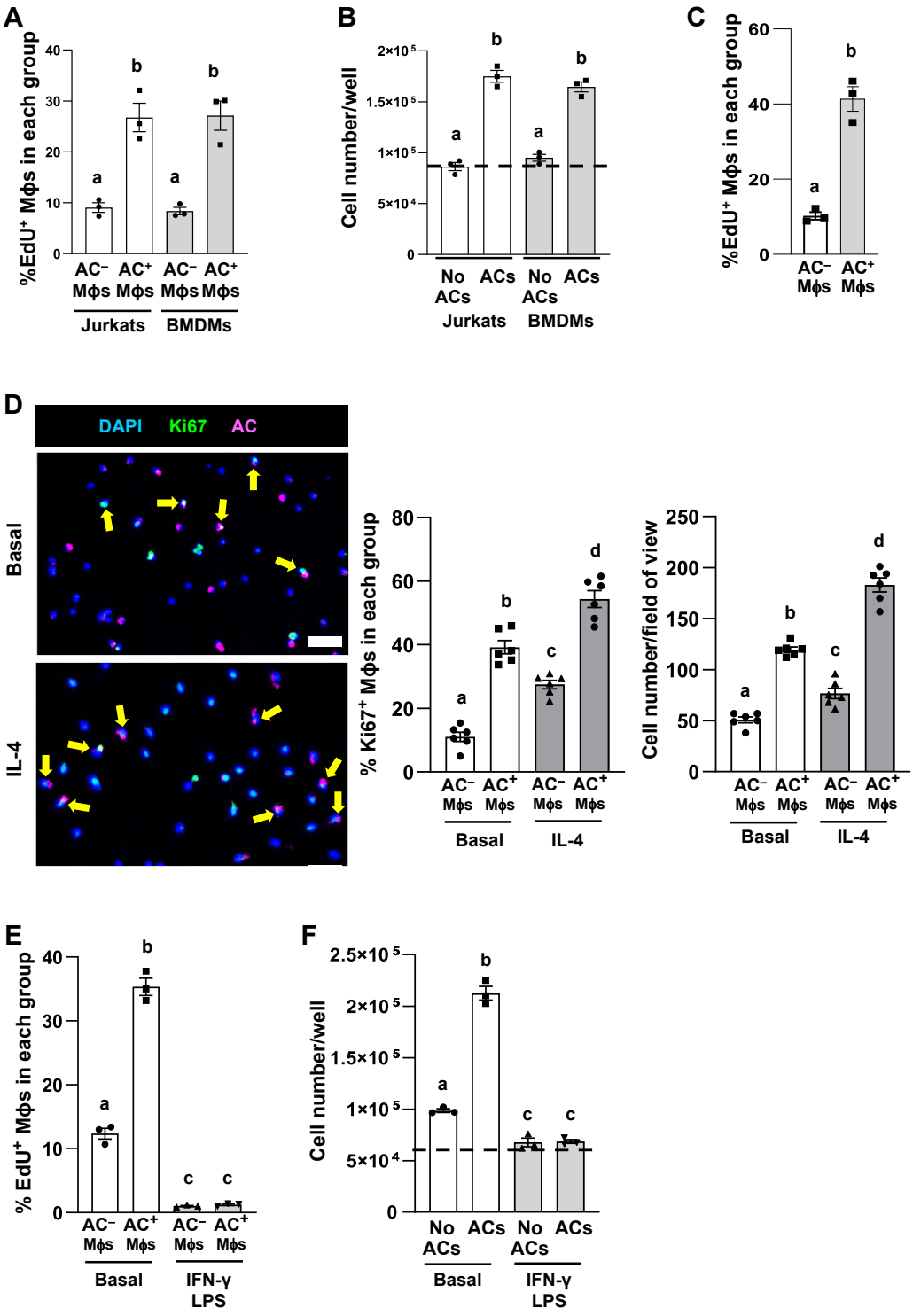
A
%EdU⁺ Mϕs in each group
AC⁻ Mϕs
AC⁺ Mϕs
AC⁻ Mϕs
AC⁺ Mϕs
Jurkats
BMDMs
B
Cell number/well
No ACs
ACs
No ACs
ACs
Jurkats
BMDMs
C
%EdU⁺ Mϕs in each group
AC⁻ Mϕs
AC⁺ Mϕs
D
DAPI
Ki67
AC
Basal
IL-4
% Ki67⁺ Mϕs in each group
Cell number/field of view
Basal
IL-4
E
% EdU⁺ Mϕs in each group
Basal
IFN-γ LPS
F
Cell number/well
Basal
IFN-γ LPS

Figure S1. Efferocytosing Macrophages Undergo Proliferation; Related to Figure 1.

(A) EdU-labeled macrophages were incubated for 45 min with DiD-labeled apoptotic Jurkat cells or apoptotic BMDMs, rinsed, and incubated for an additional 24 hours. The percentage of EdU^+ macrophages within the AC^- and AC^+ macrophage subpopulations was assayed by flow cytometry (n = 3 biological replicates).

(B) Macrophages were incubated for 45 minutes in the absence or presence of apoptotic Jurkat cells or apoptotic BMDMs, rinsed, and incubated for an additional 24 hours. Cells were detached and quantified for cell number/well; dotted line indicates cell number at the beginning of the experiment (n = 3 biological replicates).

(C) EdU-labeled macrophages were incubated for 45 min with pHrodo™-labeled apoptotic Jurkat cells, rinsed, and incubated for an additional 24 hours. The percentage of EdU^+ macrophages within the AC^- and AC^+ macrophage subpopulations was assayed by flow cytometry (n = 3 biological replicates).

(D) *Left*, Fluorescence microscopic images of untreated macrophages (Basal) (top) or IL4-treated macrophages (bottom) incubated with DiD-labeled apoptotic Jurkat cells (ACs) for 45 minutes, rinsed, and incubated for an additional 24 hours. The cells were then immunostained for Ki67 and DAPI; yellow arrows identify DiD^+ (AC^+) $Ki67^+$ macrophages. Scale bar, 50 μm. *Middle*, quantification of the percentage of $Ki67^+$ cells within AC^- and AC^+ macrophages (n = 6 biological replicates). *Right*, After similar incubations of BMDMs with DiD-labeled ACs, cell number per field of view was assessed by counting DAPI-stained AC^- and AC^+ macrophages (n = 6 biological replicates).

(E) Macrophages were treated with vehicle or IFNγ + LPS and then incubated for 45 minutes with DiD-labeled ACs, rinsed, and incubated for an additional 24 hours. The percentage of EdU^+ cells within AC^- and AC^+ macrophages was assayed by flow cytometry (n = 3 biological replicates).

(F) Macrophages were treated with vehicle or IFNγ + LPS and incubated for 45 minutes in the absence or presence of ACs, rinsed, and incubated for an additional 24 hours. Cells were detached and quantified for cell number/well; dotted line indicates cell number at the beginning of the experiment (n = 3 biological replicates).

All values are means ± SEM; letters that are different indicate statistical significance at $p<0.05$.

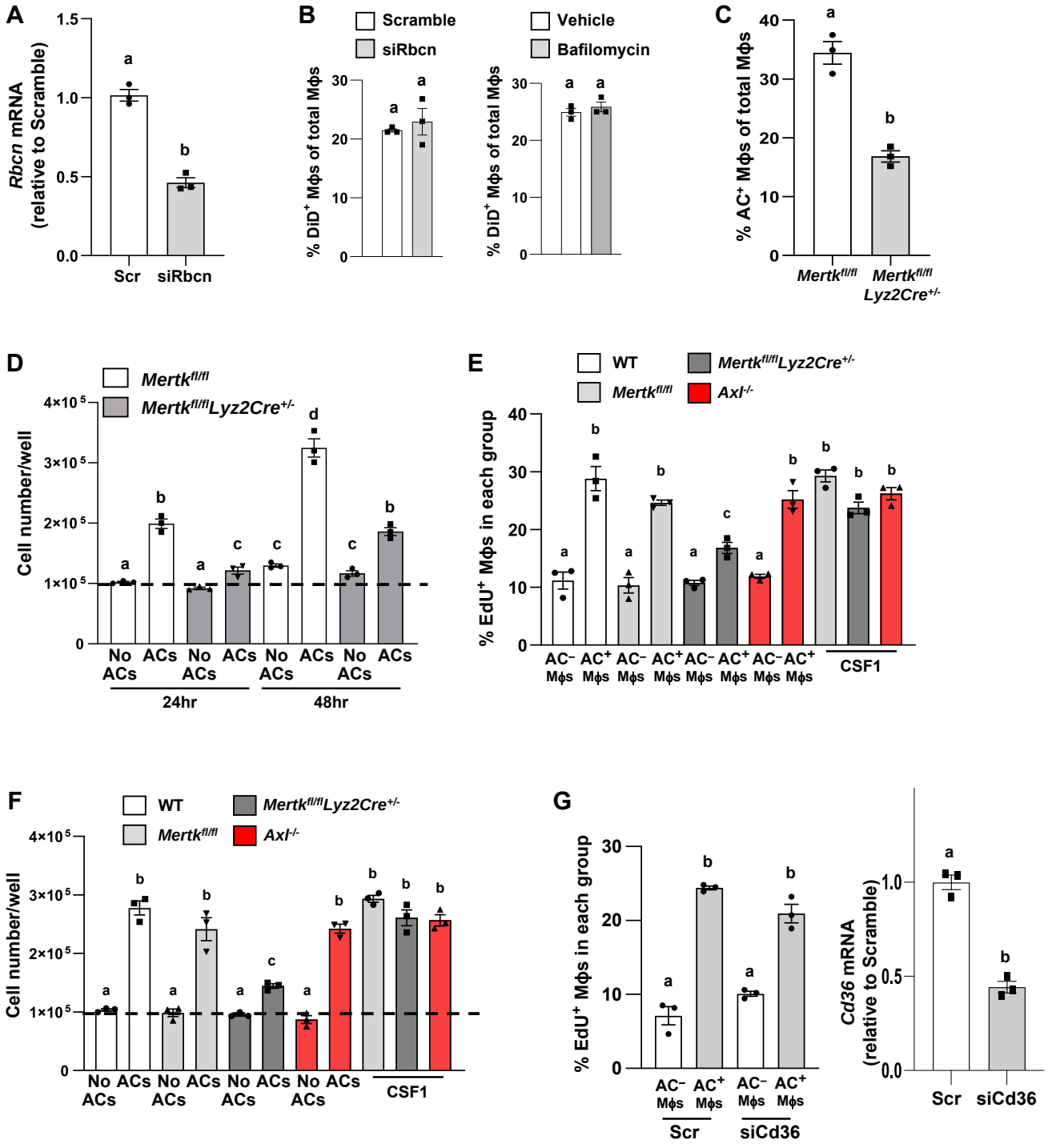
A
Rbcn mRNA (relative to Scramble)
Scr
siRbcn
B
Scramble
siRbcn
% DiD+ Mϕs of total Mϕs
Vehicle
Bafilomycin
C
% AC+ Mϕs of total Mϕs
Mertkfl/fl
Mertkfl/fl Lyz2Cre+/-
D
Mertkfl/fl
Mertkfl/fl Lyz2Cre+/-
Cell number/well
No ACs
ACs
24hr
48hr
E
WT
Mertkfl/fl
Mertkfl/fl Lyz2Cre+/-
Axl-/-
% EdU+ Mϕs in each group
AC− Mϕs
AC+ Mϕs
CSF1
F
WT
Mertkfl/fl
Mertkfl/fl Lyz2Cre+/-
Axl-/-
Cell number/well
CSF1
G
% EdU+ Mϕs in each group
Scr
siCd36
Cd36 mRNA (relative to Scramble)

Figure S2. Macrophage Proliferation Requires Phagolysosomal Degradation of ACs, with an Additional Stimulus Provided by MerTK; Related to Figure 1.

(A) Macrophages were pre-treated with scrambled RNA (Scr) or siRbcn and then assayed for *Rbcn* mRNA relative to the Scr group (n = 3 biological replicates).

(B) *Left*, Scrambled RNA- and siRbcn-transfected macrophages were incubated for 45 minutes with DiD-labeled ACs, rinsed, and quantified for the percentage of DiD^+ (AC^+) macrophages by fluorescence microscopy as a measure of AC uptake. *Right*, Macrophages treated with either vehicle or Bafilomycin A1 were incubated for 45 minutes with DiD-labeled ACs, rinsed, and quantified for the percentage of DiD^+ (AC^+) macrophages as above. For both experiments, n = 3 biological replicates.

(C) Macrophages from *Mertk*$^{fl/fl}$ and *Mertk*$^{fl/fl}$*Lyz2Cre*$^{+/-}$ mice were incubated for 45 minutes with DiD-labeled ACs, rinsed, and assayed for the percentage of DiD^+ (AC^+) macrophages by flow cytometry as a measure of AC uptake (n = 3 biological replicates).

(D) Macrophages from *Mertk*$^{fl/fl}$ and *Mertk*$^{fl/fl}$*Lyz2Cre*$^{+/-}$ mice were incubated in the absence or presence of ACs for 45 minutes, rinsed, and incubated for an additional 24 or 48 hours. The cells were then detached and quantified for cell number/well; dotted line indicates cell number at the beginning of the experiment (n = 3 biological replicates).

(E) Macrophages from WT, *Mertk*$^{fl/fl}$, *Mertk*$^{f//fl}$*Lyz2Cre*$^{+/-}$, or *Axl*$^{-/-}$ mice were labeled with EdU and either incubated with DiD-labeled ACs for 45 minutes, followed by a 24-hour incubation, or treated with CSF1 for 24 hours. The percentage of EdU^+ macrophages within each group was assayed by flow cytometry (n = 3 biological replicates).

(F) Macrophages from WT, *Mertk*$^{fl/fl}$, *Mertk*$^{f//fl}$*Lyz2Cre*$^{+/-}$, or *Axl*$^{-/-}$ mice were incubated in the absence or presence of ACs for 45 minutes, rinsed, and incubated for an additional 24 hours. The cells were then detached and quantified for cell number/well; dotted line indicates cell number at the beginning of the experiment (n = 3 biological replicates).

(G) *Left*, Macrophages were transfected with scrambled RNA or siCd36, labeled with EdU, and incubated with DiD-labeled ACs for 45 minutes, rinsed, and incubated for an additional 24 hours. The cells were assayed by flow cytometry for the percentage of EdU^+ macrophages within AC^- and AC^+ sub-populations. *Right*, *Cd36* mRNA in macrophages treated with scrambled RNA or siCd36. For both experiments, n = 3 biological replicates.

All values are means ± SEM; letters that are different indicate statistical significance at $p<0.05$.

Figure S3

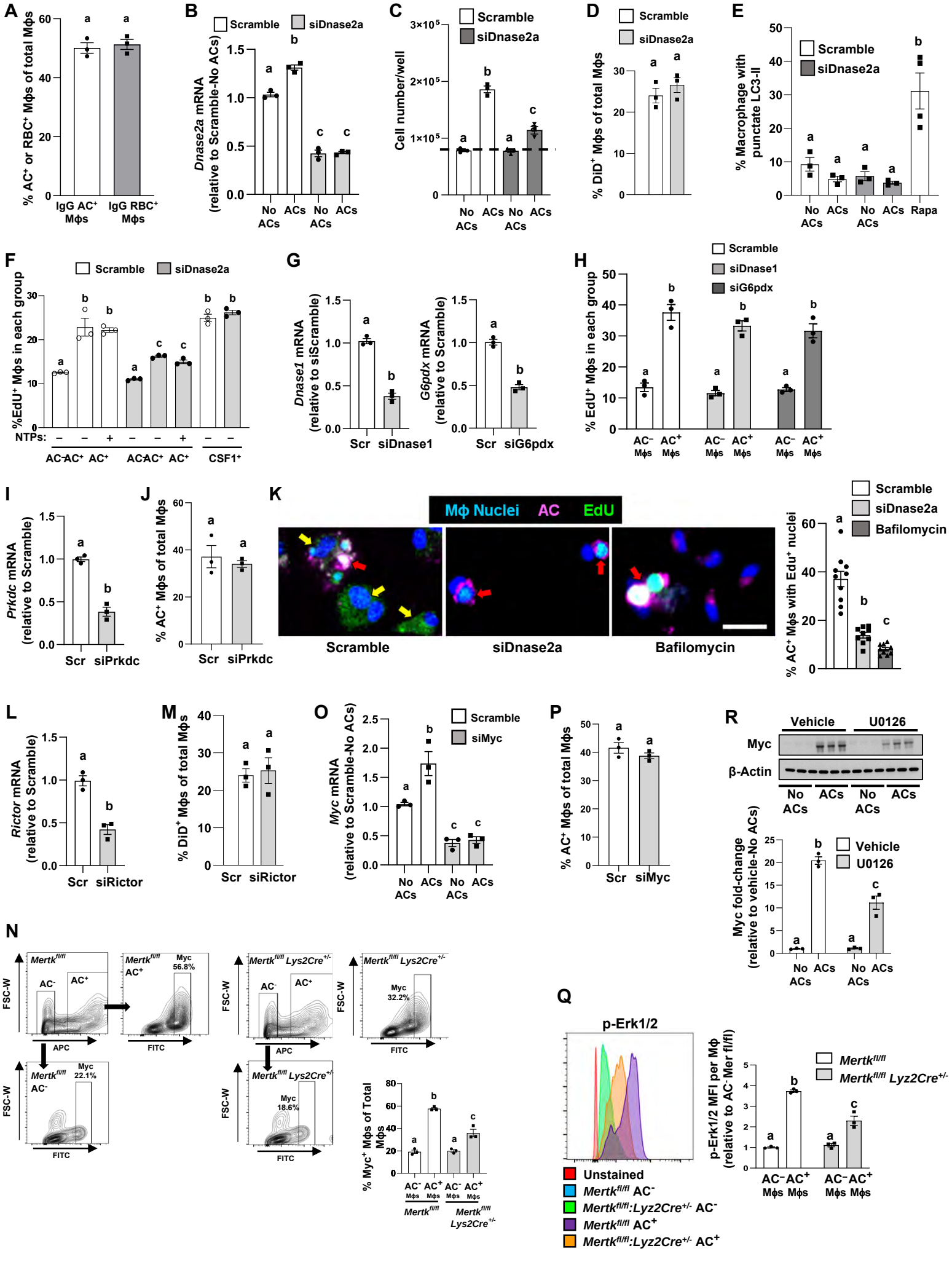
A
% AC+ or RBC+ Mφs of total Mφs
IgG AC+ Mφs
IgG RBC+ Mφs
B
Scramble
siDnase2a
Dnase2a mRNA (relative to Scramble-No ACs)
No ACs
ACs
C
Scramble
siDnase2a
Cell number/well
D
% DiD+ Mφs of total Mφs
E
Scramble
siDnase2a
% Macrophage with punctate LC3-II
Rapa
F
Scramble
siDnase2a
%EdU+ Mφs in each group
NTPs:
AC-AC+ AC+
CSF1+
G
Dnase1 mRNA (relative to siScramble)
Scr
siDnase1
G6pdx mRNA (relative to Scramble)
siG6pdx
H
Scramble
siDnase1
siG6pdx
% EdU+ Mφs in each group
AC− Mφs
AC+ Mφs
I
Prkdc mRNA (relative to Scramble)
siPrkdc
J
% AC+ Mφs of total Mφs
K
Mφ Nuclei
AC
EdU
Scramble
siDnase2a
Bafilomycin
% AC+ Mφs with Edu+ nuclei
L
Rictor mRNA (relative to Scramble)
siRictor
M
% DiD+ Mφs of total Mφs
O
Scramble
siMyc
Myc mRNA (relative to Scramble-No ACs)
P
% AC+ Mφs of total Mφs
R
Vehicle
U0126
Myc
β-Actin
Myc fold-change (relative to vehicle-No ACs)
N
Mertkfl/fl
Mertkfl/fl Lys2Cre+/-
AC-
AC+
Myc 56.8%
Myc 22.1%
Myc 32.2%
Myc 18.6%
FSC-W
APC
FITC
% Myc+ Mφs of Total Mφs
Q
p-Erk1/2
Unstained
Mertkfl/fl AC-
Mertkfl/fl:Lyz2Cre+/- AC-
Mertkfl/fl AC+
Mertkfl/fl:Lyz2Cre+/- AC+
p-Erk1/2 MFI per Mφ (relative to AC- Mer fl/fl)

Figure S3. Dnase2a and MerTK-ERK are Required for the Full EIMP Response; Related to Figures 2 and 3.

(A) Macrophages were incubated for 45 minutes with DiD-labeled IgG-coated ACs or DiD-labeled IgG-coated RBCs, rinsed, and analyzed by flow cytometry for the percentage of DiD^+ (AC^+ or RBC^+) macrophages (n = 3 biological replicates).

(B) Macrophages were transfected with scrambled RNA (Scr) or siDnase2a, incubated for 45 minutes in the absence or presence of ACs, and assayed for *Dnase2a* mRNA relative to the Scramble-No AC group (n = 3 biological replicates).

(C) Scrambled RNA- and siDnase2a-transfected macrophages were incubated in the absence or presence of ACs for 45 minutes, rinsed, and incubated for an additional 24 hours. The cells were then detached and quantified for cell number/well; dotted line indicates cell number at the beginning of the experiment (n = 3 biological replicates).

(D) Macrophages transfected with scrambled RNA or siDnase2a were incubated for 45 minutes with DiD-labeled ACs, rinsed, and assayed for the percentage of DiD^+ (AC^+) macrophages by flow cytometry (n = 3 biological replicates).

(E) Macrophages transfected with scrambled RNA or siDnase2a were incubated for 45 minutes in the absence or presence of ACs. Non-internalized ACs were rinsed away, and the macrophages were incubated for an additional 24 hours. The macrophages were fixed and immunostained using anti-LC3 with an anti-LC3A/B antibody having the strongest affinity for the LC3-II isoform (Cell Signlaing Technologies #4108S). The percent of macrophages with punctate staining was quantified. As a positive control for autophagy, one group of macrophages was treated with rapamycin (Rapa) for 18 hours (n = 3-4 biological replicates).

(F) Scrambled RNA- and siDnase2a-transfected macrophages were either incubated in the absence or presence of ACs for 45 minutes, followed by a 24-hour incubation; or treated with CSF1 for 24 hours. Some cells were treated with exogenous NTPs in the presence or absence of ACs. The cells were analyzed by immunofluorescence microscopy for the percentage of EdU^+ cells within each group (n = 3 biological replicates).

(G) Macrophages were transfected with scrambled RNA, siDnase1, or siG6pdx, incubated for 45 minutes in the absence or presence of ACs, and assayed for *Dnase1* and *G6pdx* mRNA relative to the Scr group (n = 3 biological replicates).

(H) Macrophages were transfected with scrambled RNA-, siDnase1-, or siG6pdx-transfected macrophages, labeled with EdU, incubated for 45 minutes with DiD-labeled ACs, rinsed, and incubated for an additional 24 hours. The cells were analyzed by flow cytometry for the percentage of EdU^+ cells within AC^+ and AC^- macrophages (n = 3 biological replicates).

(I) Scrambled RNA- and siPrkdc-transfected macrophages were quantified for *Prkdc* mRNA (n = 3 biological replicates).

(J) Scrambled RNA- and siPrkdc-transfected macrophages were incubated for 45 minutes with DiD-labeled ACs, rinsed, and assayed for the percentage of DiD^+ (AC^+) macrophages by flow cytometry (n = 3 biological replicates).

(K) Jurkat cells were incubated for 2 hours with EdU, then rendered apoptotic by UV irradiation, labeled with DiD. and incubated with macrophages for 45 minutes. The non-internalized ACs were then rinsed away, and the macrophages were incubated for an additional 18 hours. The cells were fixed, stained with DAPI to stain macrophage nuclei, and examined by fluorescence microscopy for EdU staining in macrophage nuclei or in residual DiD^+ AC material among macrophages that had internalized an AC. The data are quantified as the percentage of nuclei in AC^+ macrophages that were stained with EdU not associated with residual DiD^+ AC material (n = fields per condition). Yellow arrows show examples of EdU^+ macrophage nuclei., and red arrows show examples of EdU staining associated with residual DiD^+ AC material. Scale bar, 10 μm.

(L) Macrophages treated with scrambled RNA- or siRictor were quantified for *Rictor* mRNA (n = 3 biological replicates).

(M) Macrophages transfected with scrambled RNA or siRictor were incubated for 45 minutes with DiD-labeled ACs, rinsed, and assayed for the percentage of DiD^+ (AC^+) macrophages by immunofluorescence microscopy (n = 3 biological replicates).

(N) Macrophages from $Mertk^{fl/fl}$ or $Mertk^{fl/fl}$ $Lyz2Cre^{+/-}$ mice were incubated with DiD-labeled ACs for 45 minutes, rinsed, and incubated for an additional 3 hours. The cells were then immunostained for intracellular Myc and subjected to flow cytometric analysis, gating on AC^- and AC^+ macrophage (n = 3 biological replicates).

(O) Scrambled RNA- and siMyc-transfected macrophages were incubated for 45 minutes in the absence or presence of ACs, rinsed, incubated for an additional 3 hours, and quantified for *Myc* mRNA (n = 3 biological replicates).

(P) Scrambled RNA- and siMyc-transfected macrophages were incubated for 45 minutes with DiD-labeled ACs, rinsed, and assayed for the percentage of DiD^+ (AC^+) macrophages by flow cytometry as a measure of AC uptake (n = 3 biological replicates).

(Q) Macrophages from $Mertk^{fl/fl}$ or $Mertk^{fl/fl}$ $Lyz2Cre^{+/-}$ mice were incubated for 45 minutes with DiD-labeled ACs, rinsed, immunostained for intracellular p-ERK1/2, and subjected to flow cytometric analysis, gating on AC^- and AC^+ macrophages (n = 3 biological replicates).

(R) Macrophages pre-treated in the absence (Vehicle) or presence of U0126 were incubated for 45 minutes in the absence or presence of ACs, rinsed, and incubated an additional 3 hours. Lysates were immunoblotted for Myc and b-actin; the graph shows the Myc:b-actin densitometric ratio, expressed relative to the Vehicle-No AC control group (n = 3 biological replicates).

All values are means ± SEM; letters that are different indicate statistical significance at $p<0.05$.

Figure S4

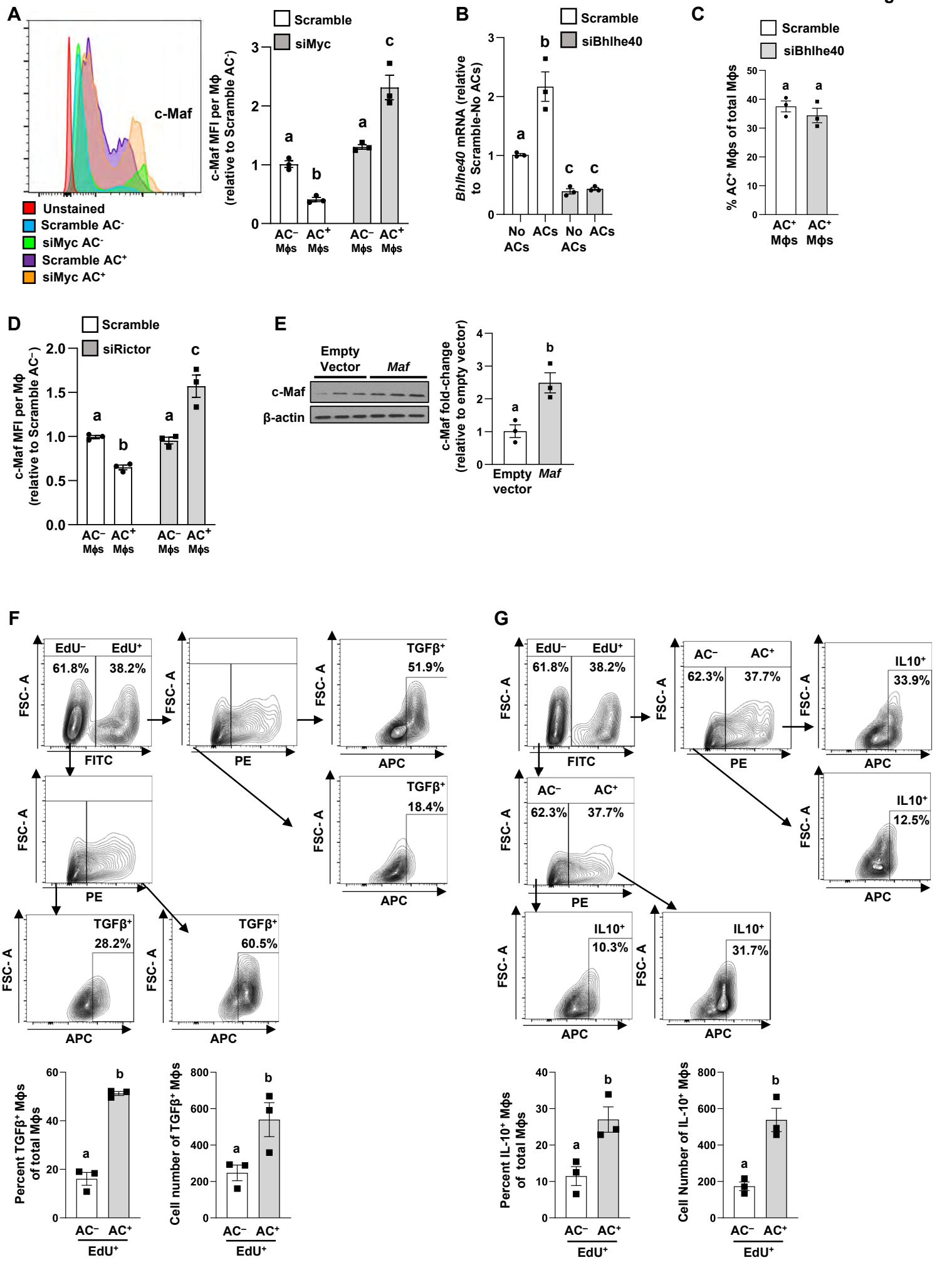
A
c-Maf
Unstained
Scramble AC⁻
siMyc AC⁻
Scramble AC⁺
siMyc AC⁺
Scramble
siMyc
c-Maf MFI per Mϕ (relative to Scramble AC⁻)
AC⁻ Mϕs
AC⁺ Mϕs
B
Scramble
siBhlhe40
Bhlhe40 mRNA (relative to Scramble-No ACs)
No ACs
ACs
C
Scramble
siBhlhe40
% AC⁺ Mϕs of total Mϕs
D
Scramble
siRictor
c-Maf MFI per Mϕ (relative to Scramble AC⁻)
E
Empty Vector
Maf
c-Maf
β-actin
c-Maf fold-change (relative to empty vector)
Empty vector
F
EdU⁻
EdU⁺
61.8%
38.2%
FSC-A
FITC
PE
APC
TGFβ⁺
51.9%
18.4%
28.2%
60.5%
Percent TGFβ⁺ Mϕs of total Mϕs
Cell number of TGFβ⁺ Mϕs
EdU⁺
G
AC⁻
AC⁺
62.3%
37.7%
IL10⁺
33.9%
12.5%
10.3%
31.7%
Percent IL-10⁺ Mϕs of total Mϕs
Cell Number of IL-10⁺ Mϕs

Figure S4. Role of Bhlhe40 and c-Maf in EIMP; and Flow Cytometry Gating Plots for Parent-Daughter Cell experiment. Related to Figures 4&5.

(A) Scrambled RNA- and siMyc-transfected macrophages were incubated for 45 minutes with DiD-labeled ACs, rinsed, and incubated an additional 6 hours. The cells were immunostained for intracellular c-Maf and subjected to flow cytometric analysis, gating on AC^- and AC^+ macrophages (n = 3 biological replicates).

(B) Macrophages were transfected with scrambled RNA or siBhlhe40, incubated for 45 minutes in the absence or presence of ACs, rinsed, incubated for an additional 6 hours, and assayed for *Bhlhe40* mRNA relative to the Scramble-No AC group (n = 3 biological replicates).

(C) Macrophages were transfected with scrambled RNA or siBhlhe40, incubated for 45 minutes with DiD-labeled ACs, rinsed, and assayed for the percentage of DiD^+ (AC^+) macrophages by flow cytometry as a measure of AC uptake (n = 3 biological replicates).

(D) Macrophages transfected with scrambled RNA- or siRictor were incubated for 45 minutes with DiD-labeled ACs, rinsed, and incubated for an additional 6 hours. The cells were immunostained for intracellular c-Maf and subjected to flow cytometric analysis, gating on AC^- and AC^+ macrophage (n = 3 biological replicates).

(E) Macrophages were transfected with empty vector or Maf-encoding plasmid. Lysates were immunoblotted for c-Maf and β-actin; the graph shows the c-Maf:β-actin densitometric ratio, expressed relative to the empty-vector control group (n = 3 biological replicates).

(F-G) Representative dot plot for the experiments in Figures 5C and 5D, showing both frequency and numbers of AC^- and AC^+ macrophages subpopulations.

All values are means ± SEM; letters that are different indicate statistical significance at $p<0.05$.

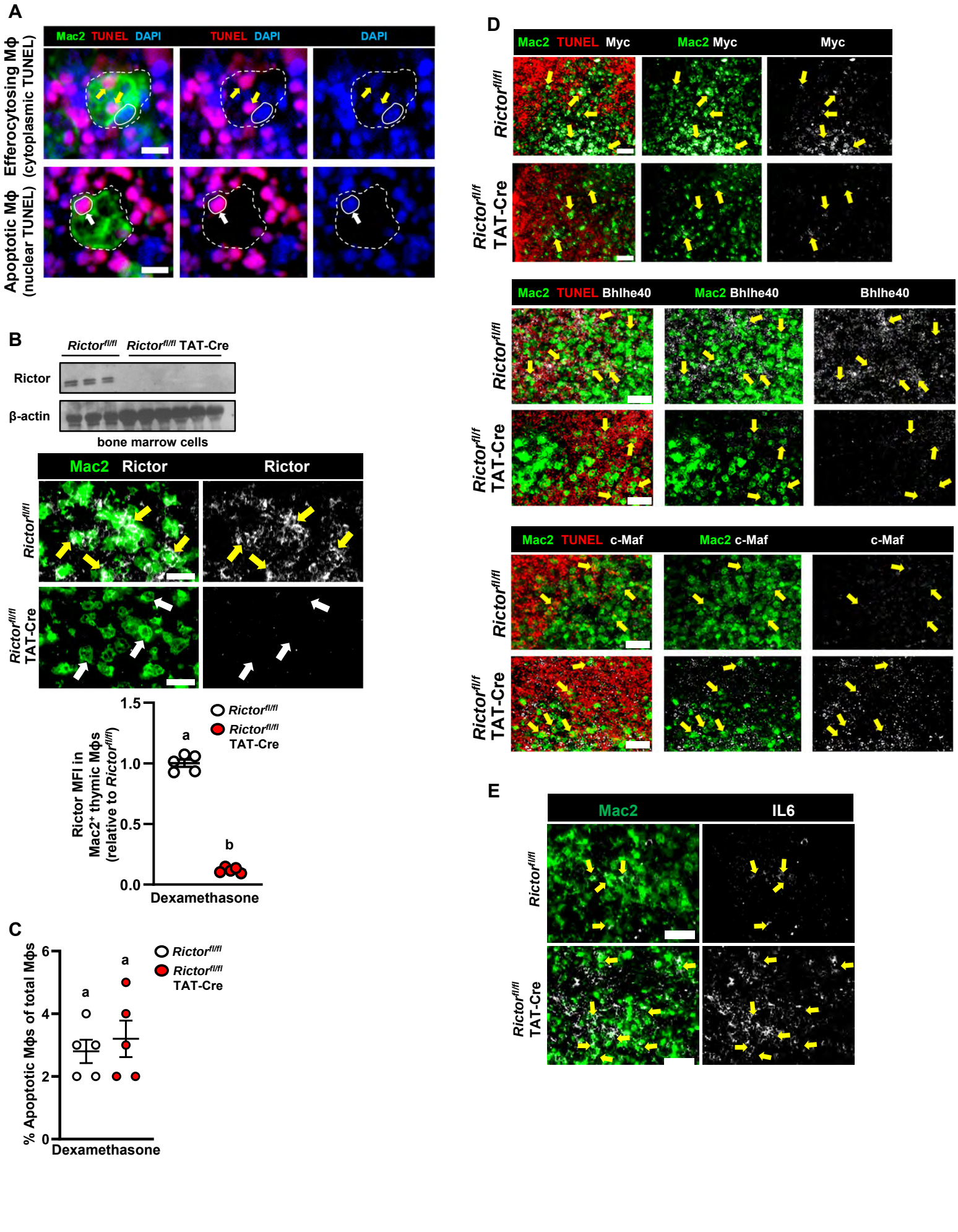
A
Efferocytosing Mϕ (cytoplasmic TUNEL)
Apoptotic Mϕ (nuclear TUNEL)
Mac2 TUNEL DAPI
TUNEL DAPI
DAPI
B
Rictorfl/fl
Rictorfl/fl TAT-Cre
Rictor
β-actin
bone marrow cells
Mac2 Rictor
Rictor
Rictorfl/fl
Rictorfl/fl TAT-Cre
Rictor MFI in Mac2+ thymic Mϕs (relative to Rictorfl/fl)
1.5
1.0
0.5
0.0
a
b
Rictorfl/fl
Rictorfl/fl TAT-Cre
Dexamethasone
C
% Apoptotic Mϕs of total Mϕs
6
4
2
0
a
a
Rictorfl/fl
Rictorfl/fl TAT-Cre
Dexamethasone
D
Mac2 TUNEL Myc
Mac2 Myc
Myc
Rictorfl/fl
Rictorfl/f TAT-Cre
Mac2 TUNEL Bhlhe40
Mac2 Bhlhe40
Bhlhe40
Rictorfl/fl
Rictorfl/f TAT-Cre
Mac2 TUNEL c-Maf
Mac2 c-Maf
c-Maf
Rictorfl/fl
Rictorfl/f TAT-Cre
E
Mac2
IL6
Rictorfl/fl
Rictorfl/fl TAT-Cre

Figure S5. Characterization of Efferocytosis and EIMP in the Thymus of Dexamethasone-Treated Mice; Related to Figure 6.

(A) *Top,* images of thymic macrophages 18 hours after i.p. injection with dexamethasone. The thymi were stained for Mac2, TUNEL, and DAPI. White dotted lines outline the macrophage cell body; solid white circle indicates macrophage nucleus. In the upper row of images, yellow arrows indicate cytoplasmic TUNEL resulting from efferocytosis of TUNEL$^+$ ACs. In the lower row of images, white arrows indicate TUNEL staining of a macrophage nucleus, illustrating a rare example of an apoptotic thymic macrophage. Scale bar, 5 μm.

(B-E) Mice were transplanted with *Rictor*$^{fl/fl}$ and *Rictor*$^{fl/fl}$ TAT-Cre bone marrow. After 4 weeks, the mice were injected i.p. with PBS or dexamethasone (Dex) and then the thymic were harvested 18 hours later.

(B) *Top,* Immunoblot of Rictor and β-actin of bone marrow lysates from the 2 groups of mice. *Middle,* images of thymic sections immunostained for Mac2 and Rictor. Yellow arrows point to macrophages expressing Rictor in the thymi of control *Rictor*$^{fl/fl}$ mice, while white arrows point to macrophages not expressing Rictor in the thymi of *Rictor*$^{fl/fl}$ TAT-Cre mice. Scale bar, 20 μm. *Bottom,* quantification of Rictor MFI in Mac2$^+$ thymic macrophages in the 2 groups of mice (n = 5 mice per group).

(C) Quantification of the percentage of apoptotic macrophages (TUNEL$^+$ nuclei in Mac2$^+$ cells) in the thymi (n = 5 mice per group).

(D) Images of thymi immunostained for Mac2, TUNEL, and either Myc, Bhlhe40, or c-Maf. Yellow arrows indicate Mac2$^+$ TUNEL$^+$ macrophages that are also positive for Myc, Bhlhe40, or c-Maf, respectively. Scale bar, 50 μm.

(E) Images of thymi immunostained for Mac2 and IL-6. Yellow arrows indicate IL6-positive area. Scale bar, 50 μm.

All values are means ± SEM; letters that are different indicate statistical significance at $p<0.05$.

Figure S6

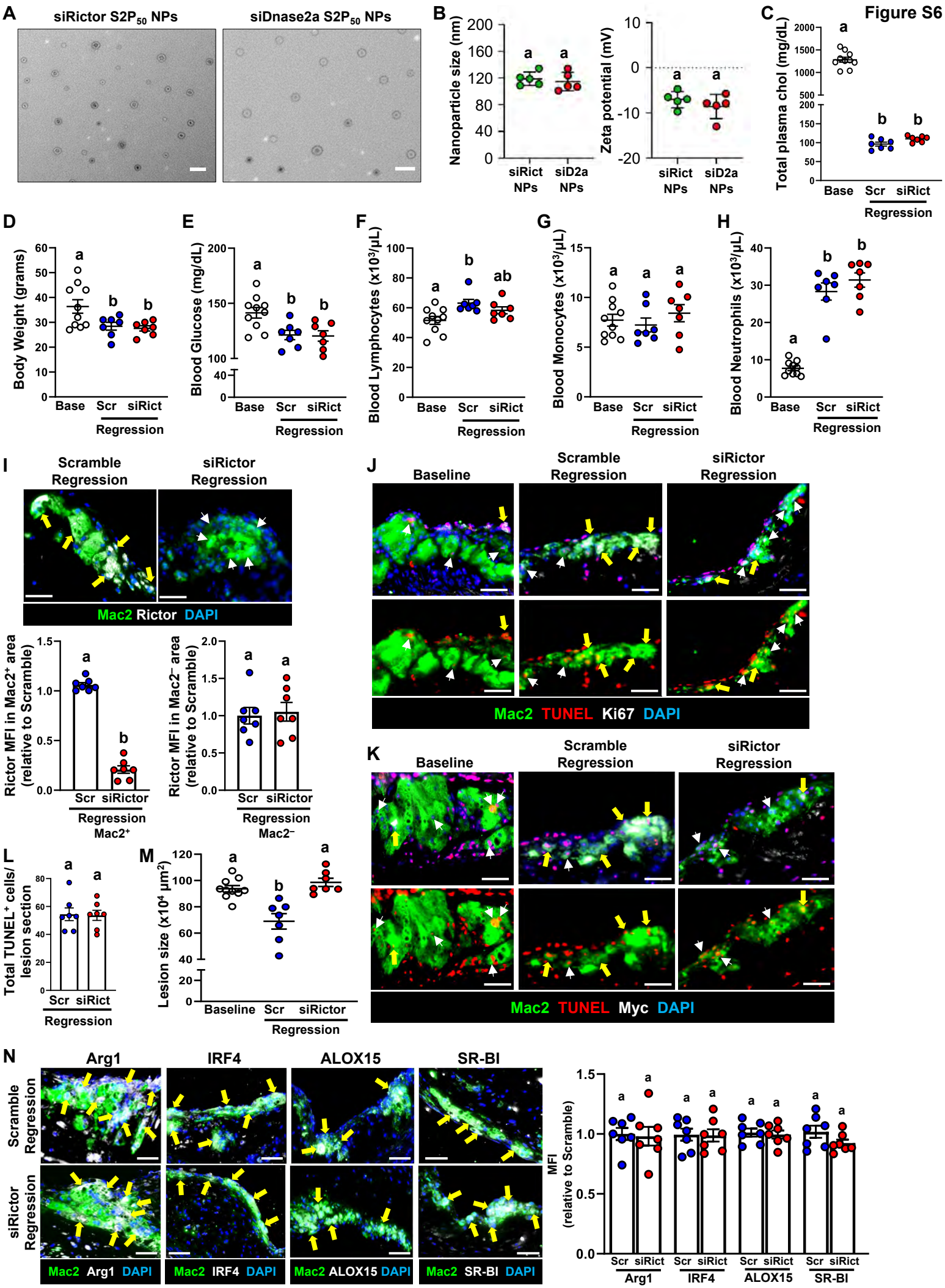
A
siRictor S2P50 NPs
siDnase2a S2P50 NPs
B
Nanoparticle size (nm)
Zeta potential (mV)
siRict NPs
siD2a NPs
C
Total plasma chol (mg/dL)
Base
Scr
siRict
Regression
D
Body Weight (grams)
E
Blood Glucose (mg/dL)
F
Blood Lymphocytes (x10³/μL)
G
Blood Monocytes (x10³/μL)
H
Blood Neutrophils (x10³/μL)
I
Scramble Regression
siRictor Regression
Mac2 Rictor DAPI
Rictor MFI in Mac2⁺ area (relative to Scramble)
Rictor MFI in Mac2⁻ area (relative to Scramble)
Scr
siRictor
Mac2⁺
Mac2⁻
J
Baseline
Scramble Regression
siRictor Regression
Mac2 TUNEL Ki67 DAPI
K
Mac2 TUNEL Myc DAPI
L
Total TUNEL⁺ cells/ lesion section
M
Lesion size (x10⁴ μm²)
Baseline
N
Arg1
IRF4
ALOX15
SR-BI
Mac2 Arg1 DAPI
Mac2 IRF4 DAPI
Mac2 ALOX15 DAPI
Mac2 SR-BI DAPI
MFI (relative to Scramble)

Supplemental Figure 6. Rictor-Dependent EIMP and Resolution in Atherosclerosis Regression; Related to Figure 7.

(A) Transmission electron microscopic images of S2P-NPs containing siRictor or siDnase2a. Scale bars, 200 nm.

(B) Size and zeta potential of siRictor (siRict) and siDnase2a (siD2a) NPs (n = 5, mean ± SEM).

(C-N) Cohorts of *Ldlr*$^{-/-}$ mice were fed the Western diet for 16 weeks and then either harvested (Baseline) or subjected to the atherosclerosis-regression protocol for 5 weeks. For the regression cohorts, the mice were administered S2P-NPs containing siRictor or scrambled (Scr) RNA at the start of the regression period (n = 7 mice per group).

(C-H) Total plasma cholesterol, body weight, fasting blood glucose, blood leukocyte counts.

(I) Immunostaining with quantification of Rictor MFI in Mac2^{+} and Mac2^{-} areas of the lesions. Yellow arrows denote macrophages with high Rictor expression and white arrows denote macrophages with low Rictor expression. Scale bars, 50 μm.

(J) Representative images of Mac2, TUNEL, and Ki67 immunostaining of DAPI-stained aortic root cross sections. Yellow arrows indicate Mac2^{+} TUNEL^{+} Ki67^{+} macrophages; white arrows indicate Mac2^{+} TUNEL^{+} Ki67^{-} or Myc^{-}. Upper row of images shows the merge, and bottom row of images show the images without the Ki67 (white) channel. Scale bars, 50 μm.

(K) Representative images of Mac2, TUNEL, and Myc immunostaining of DAPI-stained aortic root cross sections. Yellow arrows indicate Mac2^{+} TUNEL^{+} Myc^{+} macrophages; white arrows indicate Mac2^{+} TUNEL^{+} Ki67^{-} or Myc^{-}. Upper row of images shows the merge, and bottom row of images shows the images without the Myc (white) channel. Scale bars, 50 μm.

(L) Total TUNEL^{+} cells per aortic root lesion section were quantified by immunofluorescence microscopy.

(M) Aortic root lesion size.

(N) Immunostaining with quantification of Arg1, IRF4, ALOX15, and SR-BI in Mac2-stained aortic root lesions. MFI for each within macrophages was quantified by immunofluorescence microscopy and expressed relative to the mean value for the Scr regression cohort for each protein. Yellow arrows denote macrophages with Arg1, IRF4, ALOX15, and SR-BI expression, respectively. Scale bars, 50 μm.

All values are means ± SEM; letters that are different indicate statistical significance at $p<0.05$.

Figure S7

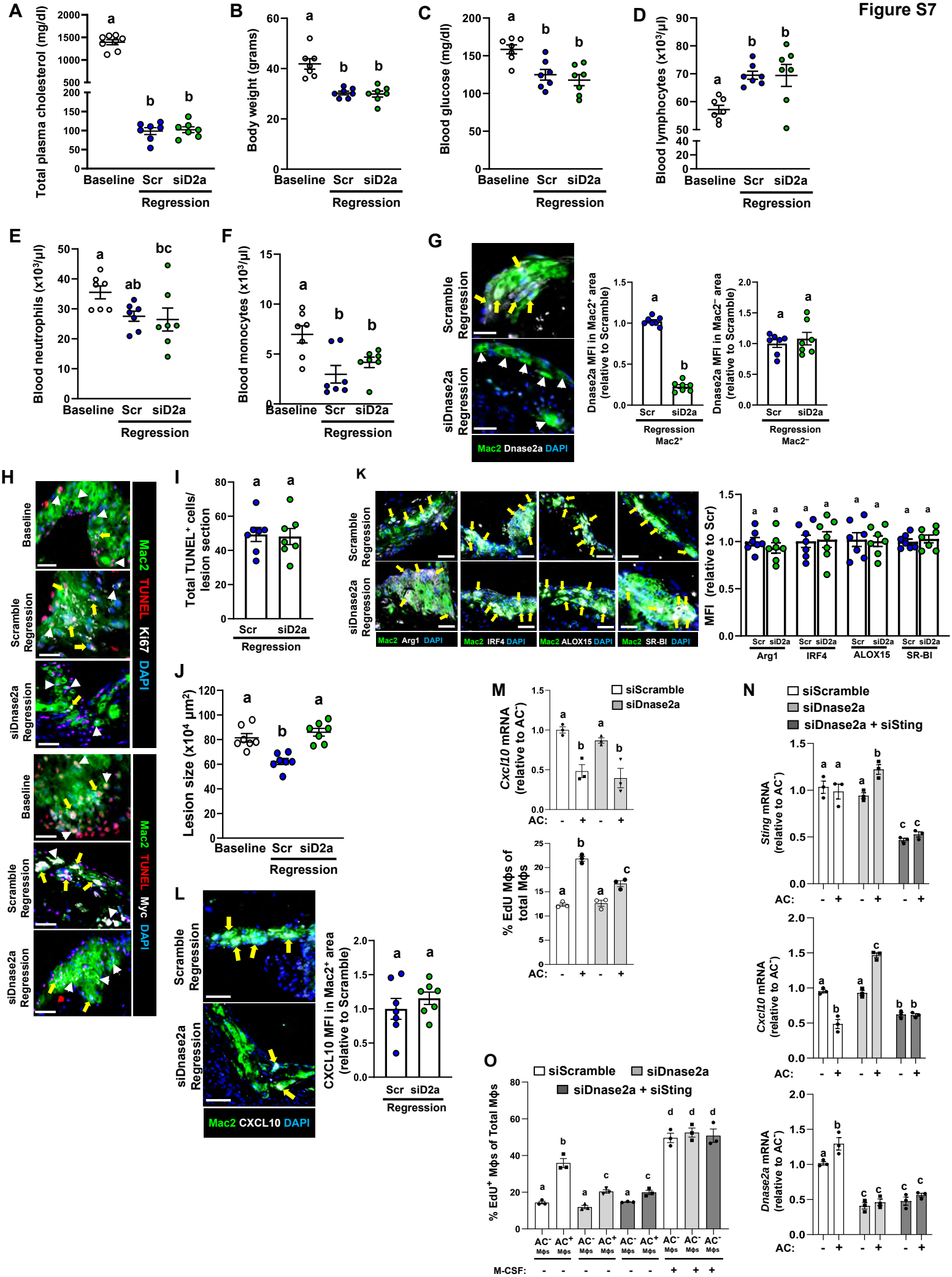
A
Total plasma cholesterol (mg/dl)
B
Body weight (grams)
C
Blood glucose (mg/dl)
D
Blood lymphocytes (x10³/µl)
Baseline
Scr
siD2a
Regression
E
Blood neutrophils (x10³/µl)
F
Blood monocytes (x10³/µl)
G
Scramble Regression
siDnase2a Regression
Mac2 Dnase2a DAPI
Dnase2a MFI in Mac2⁺ area (relative to Scramble)
Dnase2a MFI in Mac2⁻ area (relative to Scramble)
Mac2⁺
Mac2⁻
H
Mac2 TUNEL Ki67 DAPI
Mac2 TUNEL Myc DAPI
I
Total TUNEL⁺ cells/ lesion section
J
Lesion size (x10⁴ µm²)
K
Mac2 Arg1 DAPI
Mac2 IRF4 DAPI
Mac2 ALOX15 DAPI
Mac2 SR-BI DAPI
MFI (relative to Scr)
Arg1
IRF4
ALOX15
SR-BI
L
Mac2 CXCL10 DAPI
CXCL10 MFI in Mac2⁺ area (relative to Scramble)
M
siScramble
siDnase2a
Cxcl10 mRNA (relative to AC⁻)
% EdU Mφs of total Mφs
AC:
N
siScramble
siDnase2a
siDnase2a + siSting
Sting mRNA (relative to AC⁻)
Cxcl10 mRNA (relative to AC⁻)
Dnase2a mRNA (relative to AC⁻)
O
siScramble
siDnase2a
siDnase2a + siSting
% EdU⁺ Mφs of Total Mφs
AC⁻ Mφs
AC⁺ Mφs
M-CSF:

Supplemental Figure 7. Dnase2a-Dependent EIMP and Resolution in Atherosclerosis Regression; Related to Figure 7.

Cohorts of *Ldlr*$^{-/-}$ mice were fed the Western diet for 16 weeks and then either harvested (Baseline) or subjected to the atherosclerosis-regression protocol for 5 weeks. For the regression cohorts, the mice were administered S2P-NPs containing siDnase2a or scrambled (Scr) RNA at the start of the regression period (n = 7 mice per group).

(A-F) Total plasma cholesterol, body weight, fasting blood glucose, blood leukocyte counts.

(G) Immunostaining with quantification of Dnase2a MFI in Mac2^{+} and Mac2^{-} areas of the lesions. Yellow arrows denote macrophages with high Dnase2a expression and white arrows denote macrophages with low Dnase2a expression. Scale bars, 50 μm.

(H) Representative images of Mac2, TUNEL, Ki67, and Myc immunostaining of aortic root cross sections. Yellow arrows indicate Mac2^{+} TUNEL^{+} Ki67^{+} or Myc^{+} macrophages; white arrows indicate Mac2^{+} TUNEL^{+} Ki67$^{–}$ or Myc$^{–}$. Scale bars, 50 μm.

(I) Total TUNEL^{+} cells per aortic root lesion section were quantified by immunofluorescence microscopy.

(J) Aortic root lesion size.

(K) Immunostaining with quantification of Arg1, IRF4, ALOX15, and SR-BI in Mac2-stained aortic root lesions. MFI for each within macrophages was quantified by immunofluorescence microscopy and expressed relative to the mean value for the Scr regression cohort for each protein. Yellow arrows denote macrophages with Arg1, IRF4, ALOX15, and SR-BI expression, respectively. Scale bars, 50 μm.

(L) Immunostaining with quantification of CXCL10 in Mac2-stained aortic root lesions. MFI for each within macrophages was quantified by immunofluorescence microscopy and expressed relative to the mean value for the Scr regression cohort. Scale bars, 50 μm.

(M) Macrophages were transfected with scrambled RNA or siDnase2a, incubated for 45 minutes in the absence or presence of ACs, rinsed, and incubation for an additional 4 hours. The cells were assayed for *Cxcl10* mRNA relative to the scramble AC$^{–}$ group and for incorporation of EdU (n= 3 biological replicates).

(N) Macrophages were transfected with scrambled RNA, siDnase2a, or both siDnase2a and siSting, incubated for 45 minutes in the presence or absence of ACs, rinsed, and incubated for an additional 24 hours. The cells were then assayed for *Sting*, *Cxcl10*, and *Dnase2a* mRNA relative to the Scr AC$^{–}$ group (n= 3 biological replicates).

(O) Macrophages were transfected with scrambled RNA, siDnase2a, or both siDnase2a and siSting, labeled with EdU, incubated for 45 minutes with DiD labeled ACs, rinsed, and incubated for an additional 24 hours. The cells were then analyzed by flow cytometry for the percentage of EdU^{+} cells within AC^{-} and AC^{+} macrophages (n= 3 biological replicates)

All values are means ± SEM; letters that are different indicate statistical significance at $p<0.05$.